

Expected Orbit Determination Performance for the TOPEX/Poseidon Mission

R. Steven Nerem, Barbara H. Putney, J. Andrew Marshall, Francis J. Lerch, Erricos C. Pavlis, Steven M. Klosko, Scott B. Luthcke, Girish B. Patel, Ronald G. Williamson, and Nikita P. Zelensky

Abstract—The TOPEX/Poseidon (T/P) mission, launched during the summer of 1992, has the requirement that the radial component of its orbit must be computed to an accuracy of 13 cm root-mean-square (rms) or better, allowing measurements of the sea surface height to be computed to similar accuracy when the satellite height is differenced with the altimeter measurements. This will be done by combining precise satellite tracking measurements with precise models of the forces acting on the satellite. The Space Geodesy Branch at Goddard Space Flight Center (GSFC), as part of the T/P precision orbit determination (POD) Team, has the responsibility within NASA for the T/P precise orbit computations. The prelaunch activities of the T/P POD Team have been mainly directed towards developing improved models of the static and time-varying gravitational forces acting on T/P and precise models for the non-conservative forces perturbing the orbit of T/P such as atmospheric drag, solar and Earth radiation pressure, and thermal imbalances. The radial orbit error budget for T/P allows 10 cm rms error due to gravity field mismodeling, 3 cm due to solid Earth and ocean tides, 6 cm due to radiative forces, and 3 cm due to atmospheric drag. A prelaunch assessment of the current modeling accuracies for these forces indicates that the radial orbit error requirements can be achieved with the current models, and can probably be surpassed once T/P tracking data are used to fine tune the models. Provided that the performance of the T/P spacecraft is nominal, the precise orbits computed by the T/P POD Team should be accurate to 13 cm or better radially.

I. INTRODUCTION

THE joint U.S./French TOPEX/Poseidon (T/P) altimeter mission has one of the most stringent orbit determination requirements ever imposed on a satellite mission. T/P will be in a circular orbit at an altitude of 1336 km and an inclination of 66° . The orbit determination goal for T/P is to produce orbits with a radial accuracy of 13 cm root-mean-square (rms) which will provide measurements of sea level to similar accuracy. These orbits will be used for the first release of altimeter data within about a month of real time. This will require highly accurate, globally distributed tracking data as well as extremely precise models for both the gravitational and nongravitational forces acting on the satellite. The National Aeronautics and Space Administration (NASA) has selected Satellite Laser Ranging (SLR) as the nominal tracking system for its orbit determination computations. In

Manuscript received June 23, 1992; revised November 11, 1992.

R. S. Nerem, B. H. Putney, J. A. Marshall, and F. J. Lerch are with the NASA/Goddard Space Flight Center, Space Geodesy Branch, Greenbelt, MD 20771.

E. C. Pavlis is with the Department of Astronomy, University of Maryland. S. M. Klosko, S. B. Luthcke, G. B. Patel, R. G. Williamson, and N. P. Zelensky are with Hughes STX Corporation.

IEEE Log Number 9206785.

addition, tracking data from the French Doppler Orbitography and Radiopositioning Integrated by Satellite (DORIS) system will be made available to NASA. The Space Geodesy Branch at Goddard Space Flight Center (GSFC) has the responsibility within NASA, as part of the T/P precision orbit determination (POD) Team, for the precision orbit determination (POD) for T/P. In preparation for the launch of T/P during the summer of 1992, GSFC has been developing improved precision orbit determination computer software system, static and time-varying gravitational models, and nonconservative force models. This paper will summarize the progress that has been made in all aspects of precision orbit determination for T/P and review the actual orbit determination accuracies expected given the current models and expected performance of the SLR and DORIS tracking systems.

In principle, T/P contains five tracking systems which could be used for determining its orbit:

- 1) SLR [1],
- 2) DORIS Doppler tracking [2],
- 3) Global Positioning System (GPS) tracking [3],
- 4) Tracking and Data Relay Satellite System (TDRSS) tracking [4], and, as a supplementary type,
- 5) the satellite altimeter measurements themselves [48].

For the orbits NASA produces for the altimeter Geophysical Data Records (GDRs), only the SLR and DORIS data types are planned to be used, although other data types, such as GPS, may be incorporated should they become available. The GPS receiver on T/P is experimental and thus these data cannot be initially considered for inclusion in the operational precise orbit computations. Satellite-to-satellite tracking between the TDRSS satellites and T/P could be valuable if a sufficient quantity of data are collected and if the effect of the ionosphere can be modeled. While satellite altimeter data from T/P will be readily available, there is a possibility that its use to improve the orbit computations may obscure some of the oceanographic signals which T/P is trying to observe. Therefore, the altimeter data will only be employed to validate the orbit computed with the SLR and DORIS data.

The T/P Precision Orbit Determination (POD) Team at GSFC is required to provide the T/P Project at the Jet Propulsion Laboratory (JPL) with an orbital ephemeris, 10 days in length (the repeat period for the T/P orbit), within 25 working days of the end time of that 10 day segment. It is expected that it will take 3 working days for the SLR data to arrive at the Crustal Dynamics Data and Information System (CDDIS), from which the POD team receives the data. Estimates of the

TABLE I
ESTIMATED ERROR BUDGET FOR MEASUREMENTS
OF SEA LEVEL BY TOPEX/POSEIDON (1σ)

Error Source	Uncertainty (cm)
Altimeter	
Instrument Noise	2.0
Bias Drift	2.0
Media	
EM Bias	2.0
Skewness	1.0
Troposphere (dry)	0.7
Troposphere (wet)	1.2
Ionosphere	1.3
Orbit	
Gravity	10.0
Radiation Pressure	6.0
Atmospheric Drag	3.0
GM	2.0
Earth and Ocean Tides	3.0
Troposphere	1.0
Station Location	2.0
RSS Absolute Error	13.3

Earth's rotation determined from LAGEOS SLR data will be supplied by the Center for Space Research at the University of Texas at Austin (UT/CSR), which also functions as the T/P POD Verification Team. The NOAA Solar Geophysical Data Center will provide measurements of the solar activity and magnetic flux. The time frame within which DORIS tracking data will be available is uncertain at this point, so the initial T/P orbits will probably be computed with only the SLR data and the DORIS data will be included in the computations as it becomes available, with both data types supporting the final precision ephemeris.

The POD Production System (PODPS) at GSFC is a set of software which has been built around GSFC's GEODYN II orbit determination program [5] and is specifically designed for the operational production of the precision orbits for T/P. The GEODYN program computes the satellite orbit using a least squares minimization of the difference between a precise model for the satellite orbit and the satellite tracking data while adjusting the parameters defining the orbit and the forces acting on the spacecraft. The GEODYN software has undergone an extensive comparison with the UTOPIA orbit determination program at the University of Texas and they presently agree at the sub-cm level. The accuracy with which the PODPS can compute the T/P orbit will only be as good as the accuracy of the models being used to predict the motion of the satellite and the accuracy of the satellite tracking data. The error budget for the computation of the radial component of the T/P orbit is shown in Table I. The various components of the error budget have driven most of the prelaunch activities of the T/P POD Team, and the remainder of this paper will focus on the prospects of attaining the accuracies prescribed in these requirements.

The orbital motion of a satellite exhibits an integrated response to the forces generated by the inhomogeneous mass distribution on and within the Earth, the gravitational effects of the Sun, Moon, and planets, the density of the atmospheric medium it traverses, the size and orientation of the satellite

surfaces exposed to the Sun and Earth and the response of these surfaces to this incident radiation. There are many forces acting on the satellite which require consideration. The forces acting on a satellite can be characterized into two groups; conservative and nonconservative with respect to the energy of the orbital system. The gravitational forces, arising from both static and tidal contributions, act in a conservative fashion. The radiative flux from the Sun and its reradiation from the Earth in the visible and infrared spectrum significantly perturb the motion of near-Earth satellites and act in a nonconservative fashion. These satellites also travel through a rarefied atmospheric medium which needs to be modeled using atmospheric density models. For atmospheric drag, solar radiation and Earth reradiation effects, and satellite thermal imbalances, the net accelerations resulting from the interaction of light and atmospheric mass particles with each elementary surface of the spacecraft are described. Any resulting imbalances affect the energy of the orbital system thus causing nonconservative changes to the system. Extensive modeling is required for both types of forces for the precise determination of the orbits of near-Earth satellites. The POD prelaunch efforts at GSFC, of necessity, are addressing both conservative and nonconservative modeling requirements.

The T/P POD error budget (Table I) dictates that errors due to the mismodeling of the Earth's gravitational field should not exceed 10 cm rms in the radial direction. In addition, 2 cm is allocated to errors in the Earth's mass (GM) and 3 cm is allotted for radial orbit errors arising from the mismodeling of the solid Earth and ocean tides. This has necessitated considerable research on the development of improved models of the static and tidal components of the Earth's gravity field over the last 8 years. With the recent improvements in the modeling of these conservative forces, accurate modeling of the nonconservative forces acting on T/P has become increasingly important. T/P mission requirements dictate that the mismodeling of nonconservative forces due to solar radiation, Earth albedo and infrared reradiation, and spacecraft thermal imbalances produce no more than 6 cm rms radial orbit error. In addition, even though T/P is at a relatively high altitude (1336 km), 3 cm has been allocated for errors in modeling the effects of atmospheric drag on the spacecraft. Given the complex nature of the T/P spacecraft, this requirement has necessitated the development of precise nonconservative force models which take into account the satellite's complex geometry, attitude variations, and surface properties.

To some extent, these conservative and nonconservative forces can be estimated using T/P tracking data. However, the tracking measurements have their own errors and they are not ideally distributed in space and time, therefore, the T/P orbit computations will depend a great deal on the available models for the forces acting on the satellite. This paper will describe the research which has been conducted in the Space Geodesy Branch at GSFC in preparation for meeting the 13 cm radial orbit accuracy requirement for the T/P mission. In particular, new developments in modeling the Earth's gravitational field and modeling the complex nonconservative forces acting on T/P will be highlighted. The T/P error budget

will be reviewed and a prelaunch assessment of the predicted orbit determination accuracies will be summarized.

II. GRAVITY FIELD AND TIDE MODELING

A. Introduction

The predominant problem in the computation of precision orbits is the modeling of the geopotential of the Earth. The goal, set in 1983, to develop a long wavelength gravity field model capable of modeling the radial position of T/P at the 10 cm rms level, initiated a complex and long term activity at both GSFC and UT/CSR in support of the T/P mission. The Goddard Earth Modeling activities at that time had produced GEM-L2 [6], which was our best state-of-the-art long wavelength model. Covariance studies using GEM-L2 revealed gravity modeling improvements of about one order of magnitude would be required to achieve this goal.

In addition to producing accurate models of the static and time-varying geopotential for general orbit determination and geophysical modeling applications, calibrated error models of the fields are required so that the uncertainties in the fields can be propagated into ephemeris uncertainties and other geodetic parameters of interest. In particular, the covariance of the gravitational solution is calibrated to enable the reliable predication of uncertainty.

Although the observational resources available for this undertaking were similar to those used for GEM-L2, many data analysis improvements and ancillary modeling augmentations could be implemented to achieve these goals. This is no small data set; there are millions of satellite tracking observations distributed over thousands of arcs of tracking data. Because of the effort involved, the improvement was necessarily incremental. The development process was planned to proceed in three distinct phases: 1) gravity models would be developed based upon the best constants, reference frame definitions, and supporting software capabilities available to us in the 1984–1985 time frame. During this period, the software would be upgraded in preparation for the next step, which is the full iteration of the field recovery; 2) the final prelaunch model will be computed based upon the full state-of-the-art constants, reference frames, and software; 3) a postlaunch gravity model tuning phase is planned. At this writing, we are completing phase 2.

The phase 1 activities resulted in the GEM-T1 to -T3 series of solutions [7]–[9]. GEM-T1, the first model published as a result of these efforts, was complete to degree 36. GEM-T2 extended GEM-T1 to include data from 31 satellites, doubled the number of orbital arcs to nearly 1200, and utilized over 2.4 million tracking observations. The GEM-T3 model, which is complete to degree 50, combined satellite tracking data with surface gravimetry and satellite altimetry. A companion model, called GEM-T3S, was computed using only the satellite tracking data contained in GEM-T3.

Throughout all of these efforts, we have continued to develop two types of gravitational solutions: 1) those relying exclusively on satellite tracking data and 2) those formed from a combination of satellite tracking data, surface gravimetry and satellite altimetry observations. Since these models

differ in character especially in terms of both the bandwidth and the nongravitational signal contained in their data, each type of model has been used by different parts of the science community. For example, many oceanographers prefer gravitational models free of altimeter data to avoid any chance of oceanographic signal being aliased into the computed gravitational model. This strategy of producing satellite-only and combination solutions also permits a calibration of the models both with and without the contribution of local gravitational signals provided by surface gravimetry and altimetry.

The phase 2 activities introduced the constants, reference frames, and improved software modeling called for by the T/P Science Team [10]. Highlights are the use of the IERS Earth orientation series together with dynamic polar motion, improved atmospheric and tidal models, albedo, general relativity, station tectonic and tidal motions. The data will be divided into arcs much the same as in GEM-T3, but most of the tracking data will be re-edited.

The final planned phase will incorporate actual T/P tracking data in the postlaunch 6-month Verification Phase of the mission. This is because all orbits experience some resonance with specific geopotential coefficients and “frozen” orbits like T/P are especially sensitive to errors in the zonal harmonics which causes them to drift away from an exactly repeating ground track. This so-called “tuning” of the model will accommodate these and other T/P specific gravitational effects. These analyses will incorporate the first major use of the T/P specific satellite nonconservative models described later in this paper.

B. Current Status of Modeling the Earth's Static Gravitational Field

We presently use several methods to assess the orbit modeling capabilities of our gravitational fields. These approaches all rely on the veracity of the calibrated error covariance of the solutions. This requires extensive assessment of the calibration process to produce a reliable error model. The calibration of the GEM-T2 gravity model is described in Lerch [11], Lerch *et al.* [12], and Marsh *et al.* [8] based on methods described in [12]. The calibration of the GEM-T3 error covariance is described in Lerch *et al.* [9], [13]. From these analyses and other tests, a reasonably comprehensive knowledge of the characteristics of the geopotential errors has been obtained.

Using the error covariance of the gravity solution, several techniques may be used to assess the orbit errors resulting from errors in modeling the gravity field:

(1) The simplest and least computationally taxing approach, although one which has certain limitations, is to use the calibrated covariance of the gravitational solution and first order linear perturbation theory [14], [15] to assess the resulting RSS orbit positional uncertainty. The limitations of this approach are: a) since errors in estimating the initial conditions of the actual orbit are not considered, the 1 cycle-per-revolution (CPR) errors are underestimated, and b) the method is not adequate for assessing longer period orbital perturbation errors where it becomes unstable. We therefore impose a cut-off

in our evaluations, and do not consider errors arising from zonal and orbital resonance effects which have periods longer than 10 days. These shortcomings are not significant enough to eliminate the usefulness of this technique.

(2) The second approach is to perform simulations which assess gravitational modeling errors in the environment of numerical integration and a complete orbit adjustment. To do so, "clones" of the gravity models are computed. The clones are developed using an eigenvector-eigenvalue analysis of the gravity solutions. The normal matrix is orthonormalized and random noise of zero mean and unit variance is added to its eigenvectors. The resulting model, when transformed back to gravity harmonic coefficient space, approximates a field which is one standard deviation away from the original field. A drawback of using this method is that there are an infinite number of different clones which could be computed, all of which satisfy these conditions. Given that T/P has unique satellite orbital characteristics, these clones may have different amplification and cancellation of correlated orbit error effects. Therefore, we normally develop a small set of clone solutions in a Monte Carlo fashion, and evaluate the range of errors which they predict. Nevertheless, the cost of these computations limit the number of fields which can be evaluated.

Once a gravity field clone has been computed, a "truth" orbit is computed using the original gravity solution and a "perturbed" orbit is computed using the gravity field clone and simulated tracking data. The difference between the perturbed orbit and the truth orbit gives a time series of the predicted orbit errors. Fig. 1 presents the power spectra of the radial orbit errors for T/P using a GEM-T2 clone. It is clear in this figure that much of this signal is at or near 1 CPR. At longer periods, errors in principally the odd zonal harmonics are capable of producing a modulation of the 1 CPR error over the arc length. This is seen in Fig. 2 where the orbit error time series is shown and the error is seen to grow as a function of time away from the middle of the arc. This is the so called "bow-tie" error effect [16]. Use of the clone field gives a complete description of one realization of the orbit error. This method will generally give errors which are larger than predicted by method (1) due to the 1 CPR errors. However, these errors will be considerably reduced when actual T/P tracking data are used to improve the gravity model. The removal of the 1 CPR errors from the results shown in Fig. 2 provides results which are comparable with method (1).

(3) By far the most computer intensive method to gauge orbit accuracy is using GSFC's ERODYN program, which uses the gravity solution error covariance matrix and the orbit variational equations integrated over a simulated time span. A formal error propagation is computed by projecting the full gravity error covariance into all orbit parameters over time. This program has been used to verify the validity of methods (1) and (2). It has also been used to statistically project tidal errors into the T/P orbit given that these errors, unlike those due to the static gravitational field, are nonrepeating over each 10-day T/P cycle.

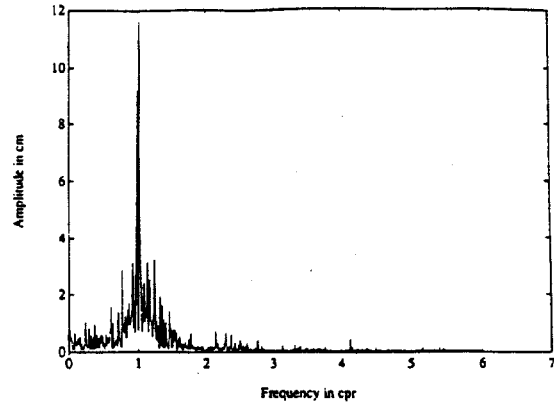


Fig. 1. Spectral characteristics of the radial orbit error for T/P using the difference of GEM-T2 "clone" model with the true GEM-T2 gravity field model.

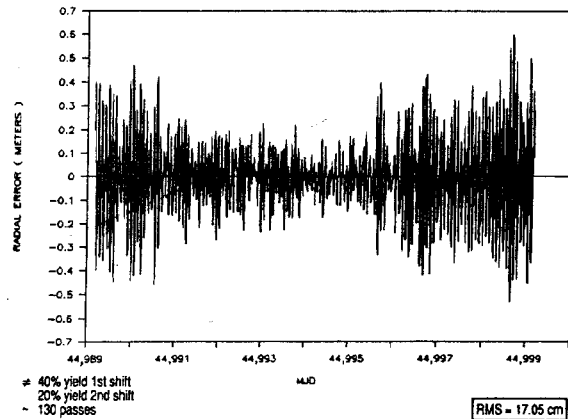


Fig. 2. Time series of the radial orbit error over 10 Days for T/P using the difference of a GEM-T2 "clone" gravity field model with the true GEM-T2 gravity field model.

(4) Finally, GSFC's orbit analysis (ORAN) program simulates a Bayesian least squares orbit adjustment. This program efficiently computes all required simulated observations and partial derivatives at an accuracy level only suitable for error analysis. It has been used mostly to assess orbit uncertainty arising from nonconservative force modeling effects. However, in tests where the gravitational error model is represented by the difference between a clone and the original GEM models, results very consistent with method (2) have been obtained.

These orbit error analysis methods all have fairly good agreement for the prediction of T/P orbit errors resulting from the mismodeling of the gravity field. We nominally use method (1) in our assessment of the orbital errors from different gravity solutions. This method does give very important information about the strengths and weaknesses of a gravitational model, especially when orbit errors are assessed within each of the individual harmonic orders of the solution.

C. Orbit Errors from the Static Gravitational Field

The Earth's gravity field is modeled as a spherical harmonic expansion of the potential as:

$$U = \frac{GM}{r} \left\{ 1 + \sum_{l=2}^{L_{\max}} \sum_{m=0}^l \left[\frac{r_e}{r} \right]^l \bar{P}_{lm}(\sin \phi) \cdot [\bar{C}_{lm} \cos m\lambda + \bar{S}_{lm} \sin m\lambda] \right\} \quad (1)$$

where

$\bar{C}_{lm}, \bar{S}_{lm}$ normalized spherical harmonic coefficients of degree l , order m ,

GM the product of the gravitational constant and the Earth's mass,

r_e the mean equatorial radius of the Earth,

$\bar{P}_{lm}(\sin \phi)$ the normalized associated Legendre function ($m \neq 0$) or the normalized Legendre polynomial ($m = 0$),

L_{\max} the maximum degree of the expansion.

Using the orbit perturbation theory [14], the gravitational field produces orbit errors which are periodic at frequencies:

$$\dot{\psi} = (l - 2p + q)(\dot{M} + \dot{\omega}) - q\dot{\omega} + m(\dot{\Omega} - \dot{\theta}) \quad (2)$$

where

l the degree of the Stokes harmonics,

m the order of the Stokes harmonics,

p a subscript in the inclination function,

q a subscript in the eccentricity function,

$\dot{\omega}$ the mean rate of the argument of perigee,

$\dot{\Omega}$ the mean node rate,

\dot{M} the mean motion rate,

$\dot{\theta}$ the mean rotation rate of the Earth.

Note that, for most altimetric missions, perigee is typically frozen and thus $\dot{\omega} = 0$. Also, perturbations fall off as $e^{|q|}$ where e is the orbit eccentricity. For near-circular satellite orbits like those used for altimetry, $q = 0, \pm 1, \pm 2$ and $p = 0 \rightarrow l$. Allowing $k = (l - 2p + q)$, the dominant errors which result are at frequencies:

$$k + m(\dot{\Omega} - \dot{\theta}) \text{ cycles/revolution.} \quad (3)$$

From (3) all terms in the geopotential model can give rise to orbital perturbations at or near 1 CPR. This is also the dominant frequency for nonconservative force model errors after the orbit adjustment process. However, the gravity model also gives rise to a more complicated error spectrum. The gravity field induces several classes of orbit perturbations. If the value of k is zero, then the resulting perturbations have a frequency of m cycles per day (" m -daily" perturbations, see Kaula [14]). If both k and m are zero, then the resulting frequency is long-period ($q\dot{\omega}$) or secular. If $k = 1, 2, 3$, etc., resonance perturbations can result with periods of 2–5 days for coefficients causing $k\dot{M} \approx m\dot{\theta}$. For other values of $k \neq 0$ short period perturbations can result with a period of one or more cycles per revolution. The gravitational error spectrum simulated for T/P has significant power at many identifiable

frequencies which arise due to errors in each of these specific classes of perturbations (Fig. 1).

The orbit error arising from the gravity model can be further segregated into that which is geographically correlated and that which is geographically variable [15], [17], [18]. The geographically correlated error is the same for repeated ascending and descending overflights of the same region. The geographically variable error, which changes sign for a satellite ascending versus descending track over a region, contributes strongly to the 1 CPR errors. At longer periods, errors in the odd zonal harmonics and resonant terms are capable of producing a modulation of the 1 CPR error over the arc length. This gives rise to errors which grow as a function of time from the middle of the arc.

The climatological model of Levitus [19] shows that the ocean dynamic topography departs significantly (± 1 m) from the geoid, and is offset in its center of figure with respect to the Earth's center of mass by as much as 15 cm [48]. The absence of perfect symmetry of the dynamic height field with respect to the geocenter gives rise to nonzero degree one terms in the spherical harmonic expansion of the dynamic height field. The degree one terms of the dynamic height field are essential for understanding long term changes in the character of the ocean circulation. $C_{1,1}, S_{1,1}$ are controlling factors in the description of the east-to-west slope of the dynamic ocean height across the major ocean basins. The $C_{1,0}$ coefficient has implications for understanding the primarily north-south seasonal thermal response of the oceans. Each of these terms has an important physical basis. It is therefore important to reduce as much as possible the orbit error contribution at 1 CPR for they are of the same spatial scale as the degree one terms in the dynamic height models.

By order, certain classes of perturbations dominate, thus one gets fairly extensive insight into the periodicities of the errors likely to be seen within the precision orbit computations. Fig. 3 compares the recent series of GEM models by their estimated T/P radial orbit uncertainty for each harmonic order. Low order m -daily perturbations and shallow orbital resonance effects are the largest contributors. An estimate of the 1σ error in the radial, along-track, and cross-track components of the T/P orbit for each of these models using the linear perturbation theory is given in Table II. Clearly, the performance of the GEM models is approaching the accuracy required for the T/P mission, with the GEM-T3 error covariance currently predicting 7 cm uncertainty for the radial component of the T/P orbit. In particular, note the comparison of the predicted T/P radial errors for the GEM-T3S model as compared to the GEM-T2 and GEM-T3 models. The GEM-T3S model predicts larger errors than GEM-T2, although the two models contain roughly the same data and the GEM-T3S model outperforms the GEM-T2 model in orbital tests. The differences in the error predictions reflects the uncertainties in our calibration of the error covariance of the solutions and is a good example of why one must use caution in the interpretation of the covariance analyses. The GEM-T3 model predicts T/P radial orbit errors which are nearly 50% better than the GEM-T3S model. This reflects the importance of satellite altimeter data and surface gravimetry in the development of GEM-T3.

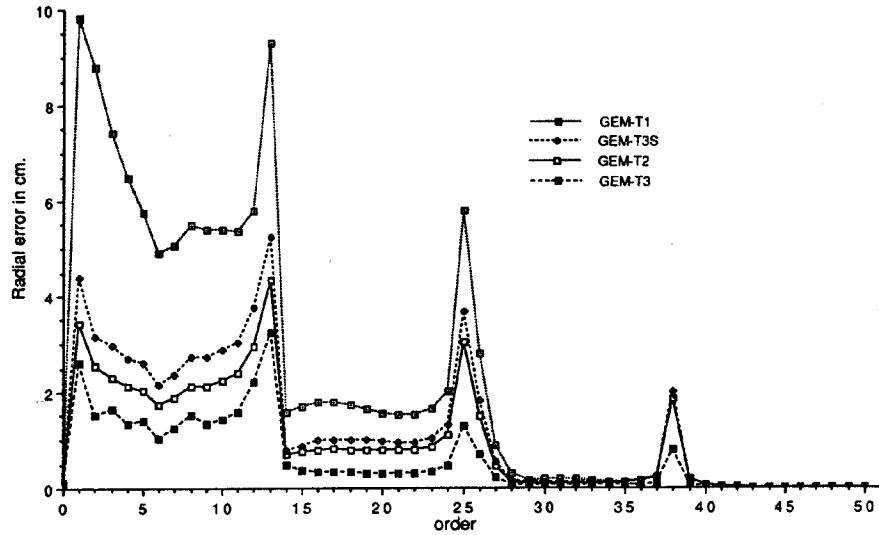


Fig. 3. Radial orbit error for T/P versus spherical harmonic order for each of the recent GEM gravitational models.

TABLE II
PREDICTED ORBIT ERROR DUE TO GRAVITY FOR TOPEX/POSEIDON (cm) 1σ

Gravity Model	Radial	Cross-Track	Along-Track
GEM-L2	65	73	262
GEM-T1	26	31	222
GEM-T2	10	15	146
GEM-T3S	13	19	175
GEM-T3	7	12	122

A comprehensive analysis of radial orbit errors using linear perturbation theory was by Rosborough [20] who developed a formulation of the radial orbit perturbations due to the geopotential as a function of latitude and longitude for near-Earth, circular orbits which is given as:

$$\Delta r(\phi, \lambda) = \sum_{l=2}^{L_{\max}} \sum_{m=0}^l \bar{Q}_{lm}^c [\bar{C}_{lm} \cos m\lambda + \bar{S}_{lm} \sin m\lambda] \pm \sum_{l=2}^{L_{\max}} \sum_{m=0}^l \bar{Q}_{lm}^s [\bar{C}_{lm} \cos m\lambda - \bar{S}_{lm} \sin m\lambda] \quad (4)$$

where the quantities \bar{Q}_{lm}^c , \bar{Q}_{lm}^s are functions of the satellite latitude, the mean orbit elements describing the satellite's orbit, and the mean rotation rate of the Earth (see [20] and [15] for a detailed description). The choice of sign for the second term in (4) is positive for an ascending pass of the satellite and negative for a descending pass. Since the radial perturbation expressed in (4) is a linear function of the geopotential coefficients, this relation can easily be used to map the error covariance of the gravity into errors in the radial component of the satellite orbit. The mean radial perturbation, found by averaging the perturbation on the ascending and descending tracks, may be written as:

$$\Delta r_m(\phi, \lambda) = \sum_{l=2}^{L_{\max}} \sum_{m=0}^l \bar{Q}_{lm}^c [\bar{C}_{lm} \cos m\lambda + \bar{S}_{lm} \sin m\lambda]. \quad (5)$$

This component of the radial orbit error is commonly called the "geographically correlated" component, since it is the same at each geographic location, regardless if the satellite is on an ascending or descending track. Another component which is of much interest to scientists processing altimeter data is the "crossover" component, which is the difference of the radial orbit perturbation where an ascending and descending track intersect and can be written as:

$$\Delta r_c(\phi, \lambda) = 2 \sum_{l=2}^{L_{\max}} \sum_{m=0}^l \bar{Q}_{lm}^s [\bar{C}_{lm} \cos m\lambda - \bar{S}_{lm} \sin m\lambda]. \quad (6)$$

The crossover component is important because it can be directly observed in the altimeter crossover measurements, whereas the geographically correlated component cannot be detected using altimetry alone.

Table III summarizes the different components of the radial orbit error for the T/P orbit using Rosborough's technique. Note that a significant component of the total radial orbit error is geographically correlated. Fig. 4 shows the geographical distribution of the mean radial orbit error for T/P using the GEM-T3 error covariance. There is considerable geographic variation due to the variation in the distribution of the tracking data contained in the GEM-T3 gravity model. This error will be reduced after the gravity model has been tuned with T/P tracking data. The DORIS tracking data will be extremely valuable for this purpose as its near global coverage will help reduce the higher orbit error shown at some of the locations in Fig. 4.

D. Iteration of the GEM-T3 Gravity Model

There is considerable margin for further improvement of the GEM gravitational models. There are many ancillary models which have been developed and tested which are now available for inclusion in the gravity model development. The existing GEM-T1, T-2, and T-3 series of models are all based on

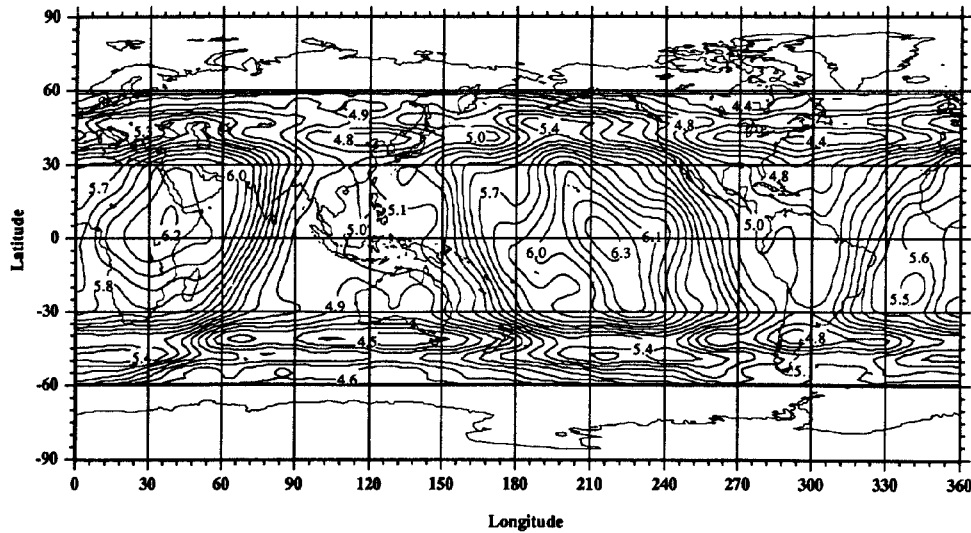


Fig. 4. Geographic distribution of the mean radial orbit error for T/P using the GEM-T3 Error Covariance Matrix.

TABLE III
PREDICTED RADIAL ORBIT ERROR DUE TO GRAVITY FOR
TOPEX/POSEIDON (cm) 1σ

Gravity Model	Total	Ascending	Descending	Mean	Cross-over
GEM-T1	26	26	26	20	36
GEM-T2	10	10	10	8	14
GEM-T3S	13	13	13	10	18
GEM-T3	7	7	7	5	9

reference parameters and geodetic models available in the 1983–1984 time frame. Over the last 5 years, the focus of our research has been on developing techniques to optimally combine data, calibrate errors, and on the orbital analysis and reduction of 1200 arcs of data. Significant changes in the constants and reference frame were not instituted over the course of developing GEM-T1 to GEM-T3 to avoid subtle inconsistencies between different geopotential solutions over time. A major iteration of the GEM-T3 gravity model was begun in the fall of 1991. Many of these improvements were implemented and represent a significant advancement over the modeling foundation used for GEM-T1 to -T3. This section will discuss the improvements which have been implemented.

The iteration activity will produce the final prelaunch static and tidal gravitational models to be used as the foundation for the postlaunch gravity field tuning with T/P tracking data. In these efforts, we have been collaborating with the Center for Space Research at the University of Texas at Austin. The resulting model will be called Joint Gravity Model (JGM)-1. The improvements adopted for the iteration are summarized below:

1) *Improved Geodetic Constants:* This new series of models will exploit improved fundamental geodetic constants (e.g., improved values for the Earth’s gravitational mass (GM), the mean equatorial radius (a_e), the flattening of the mean ellipsoid (f), etc.). The *a priori* adopted value of GM is $398600.4415 \text{ km}^3/\text{sec}^2$ [21].

- 2) *Reference Frame Definition:* For the Conventional Terrestrial Reference Frame, the IERS Reference System [22] has been adopted for the iteration of the gravity model. The rotational deformation due to polar motion (“dynamic polar motion”) and the accommodation of the secular drift of the mean figure axis are now being modeled. The kinematic motions of the tracking sites are modeled using site velocities determined by SLR [23] defaulting to NUVEL-1 [24] where SLR information is unavailable. As in all recent GEM models, 5-day average values of Earth orientation parameters will be estimated. Relativity is precisely modeled for the first time in the development of the GEM models [25], [26].
- 3) *Improved Force Modeling:* The iteration has expanded the size of the gravitational solution to be complete to degree and order 70. This extension of the model was made to accommodate higher order resonance effects. The force arising from the Earth’s absorption of solar radiation and reradiation as longwave infrared radiation is now included in the force model using a model developed by Knocke *et al.* [27]. The MSIS-86 [28] atmospheric density model and an augmented parameterization of terms to accommodate drag modeling errors have been included. There have also been significant upgrades made to the tidal modeling which will be discussed in the next section. Temporal variations of the geopotential including secular and periodic terms through degree and order 4 can be estimated in the reiterated gravity model. The introduction of these parameters will be investigated in test solutions to better accommodate long period and secular changes in the geopotential believed to be occurring due to phenomena like postglacial rebound of the Earth’s crust.
- 4) *Improved Measurement Modeling:* The kinematic motion of the tracking stations due to ocean loading is now included. In addition, improved modeling of the movement

of the tracking stations caused by the tectonic plates has now been adopted [23], [24].

- 5) *Additional Tracking Observations:* A number of new tracking sets have become available and are included in the reiterated gravity model. These include DORIS data acquired on the SPOT-2 satellite, laser ranging to Etalon 1 and 2, additional SLR data from LAGEOS, Starlette, and Ajisai, and ERS-1 SLR and altimeter observations.

The iteration of the GEM-T3 gravity model represents a very significant undertaking, with much improved *a priori* models supporting the improved isolation and recovery of the gravitational coefficients. This model will be released just prior to the launch of T/P. The error characteristics of the new model, as reflected in the error covariance matrix, are unlikely to change significantly from GEM-T3, since most of the changes between the two models has involved the improvement of background models which have little effect on the error covariance of the solution.

E. Postlaunch Gravity Field Tuning

A stringent 10 cm rms limit has been placed on the radial errors in the T/P orbit resulting from gravitational mismodeling. Since the prelaunch gravitational models lack information for satellites having the specific T/P orbital characteristics, tuning of the prelaunch gravitational field (static and tidal) using actual T/P tracking data may be essential. Tuning of the models will be one of the highest priority tasks once T/P reaches orbit. This tuning is to be accomplished through the direct incorporation of T/P observations into the geopotential models. The first 6 months of the T/P Mission will supply data supporting this model development. During this time interval, a final tuned gravity model with the required accuracy is to be developed through a collaborative effort involving GSFC, UT/CSR and the Centre National d'Etudes Spatiales (CNES, the French Space Agency). A single gravity model employing the SLR and DORIS T/P data, JGM-2, is to be produced and will be used for the operational generation of both the CNES and NASA precision ephemerides.

The amount of time available for the tuning activity will be very limited. Approximately four months of tracking data will be available for incorporation into the geopotential model. The final field and its verification is to be produced within 6 months after the launch of T/P. We have developed an analysis plan for the tuning process and have used the prelaunch time period for simulations and ancillary data analyses to indicate beforehand the likely recipe for a successful tuning activity. During the Verification Phase, gravity field validations will be completed to insure that the resulting geopotential model accuracy for T/P will meet mission requirements.

Preliminary simulations (under the previous assumption that only SLR data would be used in the tuning activity) indicate that the T/P SLR data will provide a strong base for geopotential model tuning. These results are reviewed in Table IV where the following assumptions were made:

- a) the SLR stations tracked on two staggered shifts with T/P having priority on one of the shifts. The data yields (random) was assumed to be 40%/20% on the respective

TABLE IV
PROJECTED ORBIT ERRORS BASED ON GRAVITY FIELD TUNING WITH
SIMULATED TOPEX/POSEIDON SLR OBSERVATIONS (1σ)

Gravity Model	Projected RMS Orbit Errors (cm)		
	Radial	AlongTrack	CrossTrack
GEM-T2	9.4	91.1	13.0
GEM-T2 + T/PSLR (all visibilities)	3.2	8.5	4.5
GEM-T2 + T/PSLR (realistic data yield)	6.8	20.9	8.8

high and low priority shifts for one case, and all visible passes in a second case used to represent the optimistic limit for the tuning process;

- b) the weight given to the T/P SLR data was equivalent to that of Ajisai, which is the existing SLR satellite closest to T/P in altitude and inclination;
- c) the base model used for the tuning simulation was GEM-T2;
- d) the data were reduced in 10-day arcs with 10 of them being used for the tuning simulation.

The results shown in Table IV indicate that a considerable increase in the performance of the gravity field can be expected when T/P tracking data are included in the prelaunch model.

The covariances from the tuned fields will be compared with those developed in the prelaunch phase of this activity to locate unanticipated sources of model degradation. These models will undergo extensive testing at GSFC, and the T/P orbits that are produced by these fields will be evaluated by the T/P POD Verification Team at the University of Texas. These tests will be employed to insure that the T/P-tuned solution will meet mission accuracy requirements while, at the same time, not be unnecessarily "tailored" to the T/P satellite characteristics.

F. Earth and Ocean Tide Modeling

The GSFC gravitational modeling activities have focused on developing improved models of the static gravitational field using spherical harmonic expansions which efficiently accommodate the upward continuation of the field for orbital calculations. As tracking precision has increased, the fields have increased in size and accuracy. The solutions have also improved in modeling orbit perturbations arising from long wavelength tidal effects through the direct recovery of spherical harmonic terms in the tidal expansion for major tidal constituents [7], [8], [29]. For T/P, the radial orbit errors due to the mismodeling of the Earth and ocean tides are required to be less than 3 cm rms. The tide modeling problem represents two distinct challenges: 1) to improve the long wavelength tidal terms which are in resonance with near-Earth satellites and give rise to sizeable long period orbital perturbations, and 2) to incorporate in the models a large number of tidal coefficients spanning many tide lines giving rise to a whole class of short period orbital perturbations. The selection of coefficients is made on the basis of an orbital sensitivity analysis where terms having greater than a certain orbit perturbation cutoff are included. The resulting omitted terms contribute less than some tolerable RSS effect.

1) *Solid Earth Tide Modeling*: The ocean tidal modeling and parameter recovery is made in the presence of a frequency dependent model of the solid Earth tides developed by Wahr [30]–[32]. Since the coefficients describing the ocean tides and solid Earth tides cannot be distinguished, the ocean tides are estimated in the presence of a fixed solid Earth tide model since we believe that ocean tide model is more uncertain than that of the solid Earth. However, each tidal term which is estimated accommodates ocean, atmospheric and solid Earth mass redistribution at the specific frequencies estimated.

2) *Background Ocean Tide Model: Elimination of Significant Omitted Terms*: Because of the large number of tidal terms required, an algorithm for efficiently computing all tides within a tidal family is utilized to reduce the computational burden. Using a formulation developed by Colombo [33], these expanded tidal models have been used in our current gravity field iteration and are to be used for the T/P orbital computations. The model is an advancement over that used in the development of GEM-T1 through GEM-T3 in several significant ways. The new formulation computes the tidal accelerations within each family (e.g., the mainline and narrow band of smaller sideband tides) through the direct scaling of the accelerations due to the mainline. A summary of Colombo's development is presented below:

The formulation derived in Christodoulidis *et al.* [29] show the disturbing potential arising due to the ocean tides as:

$$U = 4\pi G r_e \rho_w \sum_f \sum_{lq} \frac{(1+k'_l)}{(2l+1)} C_{la f}^{\pm} \cdot \cos\left(\sigma_f(t) \pm q\lambda + \pi - m \frac{\pi}{2} + \varepsilon_{la f}^{\pm}\right) P_{lq}(\phi) \quad (7)$$

where

- G the gravitational constant,
- r_e the average radius of the Earth,
- ρ_w the average density of sea water,
- k'_l a load deformation coefficient,
- $C_{la f}^{\pm}$ the amplitude of the tidal term in the spherical harmonic expansion,
- $\varepsilon_{la f}^{\pm}$ the phase of the tidal term,
- $\sigma_f(t)$ the astronomical phase at time, t ,
- λ the subsatellite longitude,
- m the order of the tidal species, where $m = 0, 1, 2$ are the long period, diurnal and semidiurnal tides, respectively,
- $P_{lq}(\phi)$ the Legendre function of degree l , and order q ,
- l, q the degree and order of the tidal harmonic,
- f ranges over all tidal constituents,
- \pm arises in the decomposition of the Doodson tidal argument number to a set of subscripts following Christodoulidis *et al.* [29].

This osculating element formulation assumed that the tidal amplitudes are constant, which is not a good assumption for a few of the tidal constituents which depend strongly on the lunar eccentricity. If the Earth's response is proportional to the tidal forcing, then a formulation which accounts for the

missing variation is:

$$U = 4\pi G r_e \rho_w \sum_f \left| \frac{V_f(t)}{\bar{V}_f} \right| \sum_{lq} \frac{(1+k'_l)}{(2l+1)} C_{la f}^{\pm} \cdot \cos\left(\sigma_f(t) \pm q\lambda + \pi - m \frac{\pi}{2} + \varepsilon_{la f}^{\pm}\right) P_{lq}(\phi) \quad (8)$$

where $V_f(t)$ is the amplitude of the osculating tidal forcing and \bar{V}_f is the corresponding amplitude of the mean tidal forcing (the product of the Doodson Constant and the Doodson Coefficient) for the tidal frequency f . This allows $C_{la f}^{\pm}$ to be constant and consistent with the values derived using a mean element theory. $V_f(t)$ exhibits typical changes of a few percent for most constituents, but is up to 40% for terms depending on the lunar eccentricity.

Under the assumption that the admittance of the Earth is sensibly identical at the nearby frequencies within each tidal family, Colombo took this development a step further. By taking advantage of the slow modulation of the main line tides by the sidebands, the contribution to the tidal potential of the sidebands are evaluated through a linear scaling using tidal admittances. This permits efficient computational treatment of the sideband tides. This scaling is

$$U = 4\pi G r_e \rho_w \sum_f \sum_{lq} \frac{(1+k'_l)}{(2l+1)} C_{la f}^{\pm} \left\{ \begin{array}{l} -A_f(t) \cos\left(\sigma_f(t) \pm q\lambda + \pi - m \frac{\pi}{2} + \varepsilon_{la f}^{\pm}\right) \\ +B_f(t) \sin\left(\sigma_f(t) \pm q\lambda + \pi - m \frac{\pi}{2} + \varepsilon_{la f}^{\pm}\right) \end{array} \right\} P_{lq}(\phi) \quad (9)$$

where

$$A_f(t) = \sum_j \left| \frac{V_{fj}(t)}{\bar{V}_{fo}} \right| \cos(\sigma_{fj}(t) - \sigma_{fo}(t))$$

$$B_f(t) = - \sum_j \left| \frac{V_{fj}(t)}{\bar{V}_{fo}} \right| \sin(\sigma_{fj}(t) - \sigma_{fo}(t)). \quad (10)$$

f_o represents the main tide line within the narrow constituent band and f_j identifies the individual sideband lines. The GEODYN software contains an internal table which allows inclusion of all important sideband tides for each constituent in the computation of the dynamic tidal accelerations. Table V gives the mainline Darwinian name, its Doodson number and the sideband tides forming the tidal constituent families. Other tides which require modeling for T/P orbit computations, but which lack significant sideband contributions are shown in Table VI.

Casotto [34] used an analytical orbit theory to evaluate the ocean tidal perturbations on the T/P orbit. On the basis of this study, a set of spherical harmonic coefficients for over 80 tide lines were identified as being T/P-sensitive. Many of these are sideband tides and some are tides which result from the interaction of the third bodies with one another. These latter tides are implicitly modeled in the GEODYN formulation through our use of the osculating Kepler elements of the perturbing bodies. Casotto's goal was to achieve omission errors from the ocean tides of less than 1 cm RSS radially for the T/P orbit.

TABLE V
TIDAL FAMILIES MODELED IN GEODYN II USING SCALING BASED ON ADMITTANCES

Name	Mainline		Family		
	Doodson Numbers		Doodson Numbers		
Sa	056.5545	056.5565			
Ssa	057.5555	057.5535			
Mm	065.4555	065.4755	065.6555	065.6655	065.6755
		065.6855			
Mf	075.5555	075.3355	075.3555	075.3655	075.3755
		075.5655	075.5755	075.5855	
Mtm	085.4555	085.2555	085.4655	085.4755	
Q1	135.6555	135.6355	135.6455	135.8555	
O1	145.5555	145.5455	145.7455	145.5255	145.7555
		145.7655	145.7755	145.5355	
M1	155.6555	155.4455	155.4555	155.6455	155.6655
		155.6755			
P1	163.5555	163.5575			
K1	165.5555	165.5355	165.5455	165.5655	165.5755
J1	175.4555	175.4455	175.4655	175.4755	175.6555
		175.6655			
Oo1	185.5555	185.3555	185.3655	185.5655	185.5755
		185.5855			
2N2	235.7555	235.7455			
N2	245.6555	245.6455			
M2	255.5555	255.7555	255.5455	255.7455	255.7755
L2	265.4555	265.4455	265.6455	265.6555	265.6655
		265.6755			
S2	273.5555	273.5575			
K2	275.5555	275.5455	275.5655	275.5755	
		255.7655	255.5355	255.5255	

TABLE VI
TIDES NOT HAVING SIGNIFICANT SIDEBAND TERMS

Sta	058.5545	$\phi 1$	167.5555
$\pi 1$	162.5565	-	271.5575
S1	164.5545	R2	274.5545
$\psi 1$	166.5545	-	295.5555

In our treatment of Casotto's recommendations, any coefficient requiring modeling in either the mainline or its sidebands was included in our model. We have tested Casotto's conclusions for the mainline and sideband tides using numerical experiments where a tide model complete to degree and order 15 for each constituent was used to generate a simulated T/P orbit. The orbital position over time was used as a data type and was fit with a truncated tide model containing only terms required by Casotto's analysis. The orbit errors representing the orbit misclosure in Cartesian orbital elements were mapped into their radial, cross-track and along-track components. RMS and mean orbit errors were computed for each of these test cases. These results are summarized in Table VII and confirm Casotto's analysis. However, the resulting tide model has over 1600 mainline coefficients being considered, and if one included the total size of the model considering evaluation of all the terms contained within each of the tidal families, 6000 terms are being modeled. This is the *a priori* background ocean tidal model which is used in both the gravity model iteration and T/P POD activities.

3) *Errors in the Modeled Long Wavelength Tidal Terms:* Recent Goddard Earth Models have simultaneously recovered both the static gravity field and the long-wavelength tidal field simultaneously. There are many tidal components which, while

TABLE VII
TEST OF TOPEX ORBIT ERRORS DUE TO OMITTED OCEAN TIDAL TERMS

Tide Family	Full 15 Degree and Order Harmonic Models versus Casotto [34] Designated Subset of Significant Terms			RMS Error (cm)		
	Mean Error (cm)	Radial Cross Along Trk		Radial Cross Along Trk		
Sa	0.00	0.00	0.25	0.00	0.01	0.25
Ssa	0.00	-0.03	0.18	0.06	0.24	0.78
Mtm	0.00	0.00	-0.59	0.05	0.10	0.27
Mm	0.00	-0.01	0.53	0.02	0.04	0.46
Mf	0.00	0.01	-0.36	0.10	0.07	0.38
Q1	0.00	0.00	-0.25	0.22	0.30	1.20
K1	0.00	0.00	-0.41	0.22	0.43	0.89
P1	0.00	0.02	-0.18	0.20	0.20	0.59
J1	0.00	0.00	0.17	0.05	0.08	0.27
Oo1	0.00	0.00	0.31	0.04	0.07	0.42
M1	0.00	0.00	0.32	0.01	0.01	0.26
O1	0.00	0.01	-0.07	0.26	0.37	1.14
M2	0.01	0.00	-0.46	0.42	1.40	2.76
S2	0.00	0.00	-0.05	0.25	0.42	0.99
N2	0.00	0.00	-0.73	0.24	0.35	1.19
K2	0.00	0.00	-0.00	0.18	0.24	0.76
2N2	0.00	0.00	0.24	0.17	0.14	0.62
L2	0.00	0.00	-0.05	0.09	0.11	0.33
T2	0.00	0.00	-0.10	0.05	0.06	0.24
			RSS:	0.79	1.70	4.05

being diurnal or semidiurnal on the Earth's surface (due to the Earth's rotation with respect to the perturbing sun and moon), give rise to long period orbital perturbations. Therefore, the complete tide model from recent GEM solutions contains both adjusted and unadjusted terms.

TABLE VIII
TOPEX/POSEIDON ORBIT ERRORS FROM ERRORS
IN THE LONG-WAVELENGTH OCEAN TIDES

Tide Model	Project RMS Orbit Errors (cm)		
	Radial	Along-Track	Cross-Track
GEM-T3	3	9	7

We have taken the error covariance of the GEM-T3 tide model and performed a formal propagation of the tidal errors into simulated T/P orbits. Note, since the tides have long period effects, they may interact differently over the course of the T/P Mission. However, the results shown in Table VIII are believed to be representative and indicate that prelaunch tidal modeling performance for this most critical subset of the tidal constituents, is near to the goals established for these models. Tuning of the tide model with T/P tracking data should enable us to satisfy the error budget goal of 3 cm radially from tides.

III. NONCONSERVATIVE FORCE MODELING

A. Introduction

Until recently, gravity field mismodeling was the major source of error in precise orbit computations. However, with recent improvements in these models, accurate modeling of the nonconservative forces has become a significant concern. Because the T/P mission requirements dictate that the mismodeling of the nonconservative forces of solar radiation, Earth albedo and infrared reradiation, and spacecraft thermal imbalances produce in combination no more than a 6 cm radial RMS error, the development of nonconservative force models which take the satellite's complex geometry, attitude, and surface properties into account were required. Specifically, for T/P, a "box/wing" satellite model has been implemented.

B. TOPEX/Poseidon Attitude/Yaw Steering

The T/P spacecraft has an intricate attitude control system due to its large, single axis gimballed solar array. Perfect solar pointing (sun incidence vector normal to the solar array) requires the spacecraft to yaw about its Earth-pointing Z-axis at rates which exceed the capabilities of the attitude control system. Therefore, a sinusoidal yaw command was implemented which achieves near perfect solar pointing while remaining within attitude control system limits [35]. The algorithm is based on the coordinate systems shown in Figs. 5 and 6. The spacecraft body-fixed system origin is within the vehicle body, although not at the center of mass, with the positive Y-axis pointing opposite of the solar array axis, the positive Z-axis directed to the Earth nadir, and the positive X-axis orthogonal to the Y and Z axes to complete the right-handed system. The inertial system is centered at the geocenter with the X_o-axis normal to the satellite orbit plane, the Z_o-axis points in the direction of the sun as projected into the orbit plane, and the Y_o-axis normal to these axes. As shown in Fig. 6, β' refers to the angle between the sun vector and the orbit plane and Ω is the orbit angle, measured from the Y_o-axis. The actual yaw angle, Ψ, of the spacecraft is rotated positively from the X_p-axis (the along-track direction) about

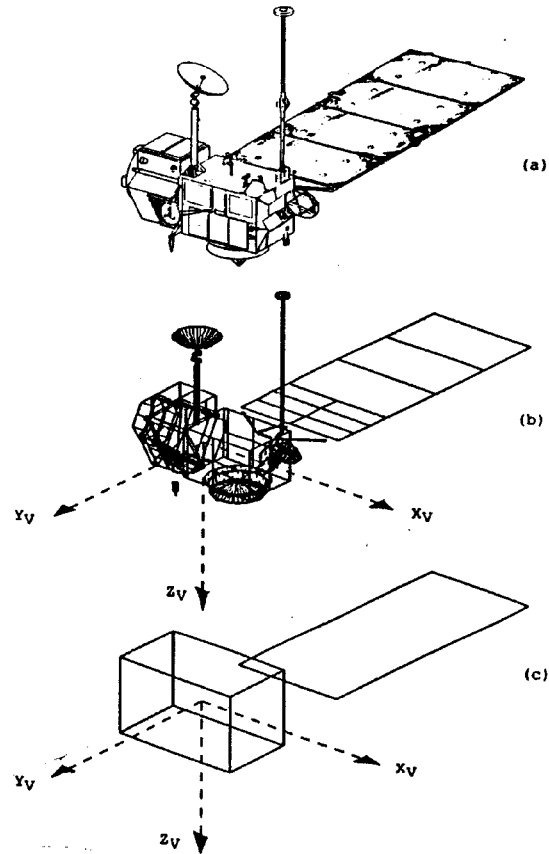


Fig. 5. (a) The TOPEX/Poseidon Spacecraft, (b) micro-model approximation, (c) macro-model approximation.

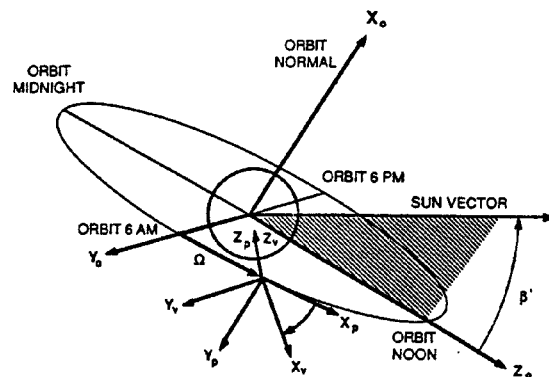


Fig. 6. TOPEX/Poseidon inertial coordinate system from Perrygo [35].

the Z-axis and is determined from the β' and Ω. The satellite is required to follow multiple yaw steering algorithms during its orbit [36]. The solar array pitch angle, γ, rotates positively from the spacecraft X-axis about the Y-axis to orient the cells toward the sun for optimum sun pointing.

C. Model Development

The first step in a detailed analysis of the radiation forces acting on T/P was to accurately compute the radiation forces

due to the Sun, Earth albedo, Earth infrared, and spacecraft thermal emissions upon T/P with the use of a finite element model of the spacecraft. This investigation generated what is referred to as the "micromodels". These acceleration histories in the radial, along-track, and cross-track directions were generated for each of the radiative forces; a thorough explanation of this modeling effort is given by Rosborough *et al.* [37], Antreasian and Rosborough [38], and Antreasian [39]. Since a precise thermal and radiative model of a spacecraft is necessarily computationally intensive, this micromodel, which served as our "truth" model, was computed off-line by the Colorado Center for Astrodynamics Research (CCAR) at the University of Colorado [39]. CCAR functions as the T/P POD Modeling Center. A relatively simple and less computationally intensive "macro-model," more suitable for precision orbit computations, was devised and tested to emulate the micro-model accelerations. This development was introduced in Marshall *et al.* [40]. A graphical representation of this modeling is shown in Fig. 5.

All of the macro-models described herein have been implemented in the GEODYN orbit determination software [5]. The results presented use GEODYN and the T/P macro-models to simulate a 10 day T/P orbit. Marshall *et al.* [41] gives a comprehensive discussions of results for all of the radiative forces acting on T/P.

The satellite shape is approximated as a combination of flat plates. The nonconservative forces acting on each of the composite surfaces are computed independently. All plate interaction effects, such as shadowing, reflection, and conduction are ignored. The model yields vector accelerations which are summed to compute the total effect on the spacecraft center-of-mass. The algorithm includes the ability to adjust aggregate parameters associated with each flat plate to obtain a better fit to the actual satellite acceleration history based on orbit errors sensed from laser tracking data and from telemetered satellite on-orbit temperatures. For T/P, a box/wing shape was chosen with the plates aligned along the satellite body-fixed coordinate system (Fig. 5).

1) *Atmospheric Drag:* The acceleration of the spacecraft caused by its interaction with the Earth's atmosphere can be described using the following equation:

$$\bar{F}_D = -\frac{1}{2} C_D \frac{A}{m} \rho(h) V_r \bar{V}_r \quad (11)$$

where

- C_D satellite drag coefficient,
- A satellite cross-sectional area projected normal to \bar{V}_r ,
- m satellite mass,
- $\rho(h)$ atmospheric density at the altitude h ,
- \bar{V}_r satellite velocity relative to the atmosphere.

Because of T/P's high altitude (1336 km) and the corresponding relatively low atmospheric density, drag is not anticipated to be a significant modeling problem. Nonetheless, the existing satellite drag model used in GEODYN has been updated to take into account the spacecraft's complex geometry and orientation. The cross-sectional area has been modified as

follows:

$$A = \sum_{i=1}^N A_i \cos \theta_i \quad (12)$$

where

- N the number of plates,
- A_i area of the i th plate,
- θ_i angle between the i th plate normal and satellite velocity vector.

Simulations have shown that his model should be adequate in order to meet the 3 cm T/P radial error mission requirement for atmospheric drag mismodeling.

2) *Solar and Earth Radiation:* Solar, albedo, and infrared emissions are the three external radiative fluxes acting on a spacecraft. The radiation pressure acting on a flat plate can be computed using the following equation [42], assuming a Lambertian diffusion:

$$\bar{\Gamma} = \frac{-GA \cos \theta}{Mc} \left[2 \left(\frac{\delta}{3} + \rho \cos \theta \right) \bar{n} + (1 - \rho) \bar{s} \right] \quad (13)$$

where

- Γ radiation pressure acceleration on the flat plate,
- A surface area of the flat plate,
- θ angle between surface normal and source vectors,
- G radiation flux from source,
- \bar{n} surface normal vector,
- \bar{s} source incidence vector,
- ρ specular reflectivity (percentage of total incoming radiation),
- δ diffusive reflectivity (percentage of total incoming radiation),
- M satellite mass,
- c speed of light.

The adjustable parameters for each plate are the area and the specular/diffusive reflectivity. These parameters are averaged values which represent the consolidated effect of the spacecraft's complex shapes and material properties.

The albedo and infrared accelerations use a similar acceleration equation to the solar radiation. However, the source vector is the Earth grid spot-to-satellite vector rather than the solar incidence vector. The spot definition and location are defined by Knocke and Ries [43]. Note that this model is not self-shadowing. The total albedo/infrared acceleration is expressed as:

$$\bar{\Gamma} = - \sum_i^N \sum_j^{19} \frac{G_j A_i \cos \theta_{ij}}{Mc} \cdot \left[2 \left(\frac{\delta_i}{3} + \rho_i \cos \theta_{ij} \right) \bar{n}_i + (1 - \rho_i) \bar{s}_j \right] \quad (14)$$

where

- i plate of interest,
- j Earth spot of interest,
- N total number of plates

and the subscripted variables are analogous to those of (11), but refer explicitly to the i th plate.

3) *Spacecraft Radiation*: Two separate types of fluxes affect the flat plate temperatures: internal and external. Internally, the equipment dissipates heat. Externally, the solar radiation, albedo, and infrared fluxes cause surface heating. The force exerted on a surface due to thermal emission, assuming a Lambertian diffusion function, can be expressed as:

$$\bar{F} = -\frac{2A\sigma}{3c}\epsilon T^4 \bar{n} \quad (15)$$

where

- ϵ emissivity,
- σ Stefan-Boltzmann constant (5.67×10^{-8} W/m²/K⁴),
- A surface area,
- T temperature (K),
- c speed of light (m/s),
- \bar{n} surface normal vector.

The temperature history algorithm, however, is difficult to model. One must take into account the complexities of 1) occultation effects, 2) oblique illumination, and 3) the spacecraft's thermal inertia, without losing sight of the need for simplicity and generality. The temperature for a surface exposed to sunlight is modeled using simple exponential heating as:

$$T = a + c \cos\left(\frac{\theta}{x}\right) \left[1 - \exp\left(-\frac{t_1}{f}\right)\right] \quad (16)$$

and in shadow using simple exponential cooling as:

$$T = a + c \exp\left(-\frac{t_2 + s_2}{d}\right) \quad (17)$$

where

$$s_2 = -d \ln\left(\cos\left(\frac{\theta_{shd}}{x}\right) \left[1 - \exp\left(-\frac{t_1}{f}\right)\right]\right) \quad (18)$$

and

- a cold equilibrium temperature,
- c delta temperature between cold and hot equilibrium,
- d transition time from hot to cold equilibrium temperature,
- f transition time from cold to hot equilibrium temperature,
- x rotation rate/thermal inertia constant,
- t_1 time since shadow exit,
- t_2 time since shadow entry,
- s_2 shift parameter to ensure continuity,
- θ angle between surface normal and solar incidence,
- θ_{shd} angle between normal and sun vectors at shadow entry.

The shift terms are functions of the satellite's temperature history, and are required to enforce continuity in temperature, a fundamental physical requirement. The adjustable parameters are area, emissivity, and all five temperature terms (a, c, d, f, x).

Note that solar radiation is the only direct effect influencing the temperature. That is to say, the θ angle and the time parameters are based only on solar illumination and neglect the albedo and infrared effects. However, albedo and infrared do indirectly influence the *a priori* values of all the adjustable

temperature parameters. A plate's orientation with respect to the sun dictates which temperature algorithm to use. The cosine term in the sunlight equation allows for the fact that an obliquely illuminated plate will have a lower temperature than one perpendicular to the sun vector. In contrast, a plate's cooling pattern, when occulted by either the Earth or the spacecraft, is independent of the sun position and, therefore, no such allowance needs to be made. The x parameter in the denominator of the cosine term accounts for the fact that the temperature is not directly proportional to the rate at which spacecraft rotation moves a plate from direct to oblique illumination. Without x , there is no delay in reaching the cold equilibrium value as the plate enters shadow. The exponential term addresses the occultation transition effects. After a face enters or leaves shadow, its changing temperature can be approximated by an exponential curve. A different time constant (d or f) is applied depending on whether the surface is heating or cooling. Finally, a shift term is introduced to ensure continuity in the transition from the sunlight to shadow temperature equation. This assumes that the plate will reach its cold equilibrium temperature in shadow before heating begins. Given that this assumption is not true, a different set of shift parameters must be established. For example, during sinusoidal yaw the X- face of T/P is occulted only by the Earth. As β' increases, this shadow time gradually decreases. Therefore, the plate will always reach its hot equilibrium temperature and not necessarily reach its cold equilibrium temperature. In this case, the following temperature history algorithms are used:

Sunlight:

$$T = a + c \cos\left(\frac{\theta}{x}\right) \left[1 - \exp\left(-\frac{(t_1 + s_1)}{f_i}\right)\right] \quad (19)$$

where

$$s_1 = -f \ln\left[1 - \exp\left(\frac{t_2}{d}\right) \left(\frac{\cos \theta_{shd}}{\cos \theta_{sun}}\right)\right] \quad (20)$$

Shadow:

$$T = a + c \cos \exp\left(-\frac{t_s + s_2}{d}\right) \quad (21)$$

where

$$s_2 = -d \ln \cos\left(\frac{\cos \theta_{shd}}{x}\right) \quad (22)$$

and

- s_1 shift parameter to ensure continuity,
- θ_{sun} angle between normal and sun vectors at shadow exit.

More simplistic representations have been tried with varying success. However, they all fail to replicate certain thermal behaviors exhibited by the micromodel. A model of this complexity is the minimum necessary to meet T/P mission requirements and is the chosen parameterization for T/P modeling.

TABLE IX
NONCONSERVATIVE FORCES MODELABILITY AND ERROR ANALYSIS SUMMARY

FORCE	RMS of Micro Model Force for β' of 0° to 88° and Orbit Angle of 0° to 360°	RMS of Macro-Micro Model Residuals	RMS Radial 10 Day Orbit (For All Components)
Solar Along Track	$3.2 \times 10^{-8} \text{ m/s}^2$	$4.3 \times 10^{-9} \text{ m/s}^2$	
Solar Cross Track	$4.5 \times 10^{-8} \text{ m/s}^2$	$4.2 \times 10^{-9} \text{ m/s}^2$	
Solar Radial	$2.7 \times 10^{-8} \text{ m/s}^2$	$4.9 \times 10^{-9} \text{ m/s}^2$	
Total Radial Orbit Error for 10 Day Arc			5.1 cm
Albedo Along Track	$6.1 \times 10^{-10} \text{ m/s}^2$	$2.3 \times 10^{-10} \text{ m/s}^2$	
Albedo Cross Track	$8.3 \times 10^{-10} \text{ m/s}^2$	$3.3 \times 10^{-10} \text{ m/s}^2$	
Albedo Radial	$4.6 \times 10^{-9} \text{ m/s}^2$	$2.4 \times 10^{-10} \text{ m/s}^2$	
Total Radial Orbit Error for 10 Day Arc			2.1 cm
IR Along Track	$6.1 \times 10^{-10} \text{ m/s}^2$	$5.4 \times 10^{-10} \text{ m/s}^2$	
IR Cross Track	$7.4 \times 10^{-10} \text{ m/s}^2$	$5.3 \times 10^{-10} \text{ m/s}^2$	
IR Radial	$5.6 \times 10^{-9} \text{ m/s}^2$	$5.4 \times 10^{-10} \text{ m/s}^2$	
Total Radial Orbit for 10 Day Arc			2.2 cm
Thermal Along Track	$2.0 \times 10^{-9} \text{ m/s}^2$	$1.0 \times 10^{-9} \text{ m/s}^2$	
Thermal Cross Track	$3.6 \times 10^{-9} \text{ m/s}^2$	$5.9 \times 10^{-10} \text{ m/s}^2$	
Thermal Radial	$1.6 \times 10^{-9} \text{ m/s}^2$	$5.5 \times 10^{-10} \text{ m/s}^2$	
Total Radial orbit Error for 10 Day Arc			5.2 cm

C. Modelability and Error Analysis

In order to test the validity of these macro-models, a comparison has been performed between the acceleration histories predicted by the macro and micromodels. A Bayesian least squares estimation procedure has been used to tailor the adjustable macromodel parameters to better fit the micromodel generated acceleration histories for the solar radiation and the thermal imbalance nonconservative forces [40]. *A priori* values with realistic uncertainties served to constrain some highly correlated parameters which could not be recovered independently. Specifically, the solar array parameters were not adjusted since their properties are relatively well known and they do not represent an average of many smaller surfaces of varying characteristics. In addition, to ensure realistic temperature values, the equilibrium temperatures, a and c , were constrained so as not to stray more than a few degrees from the values predicted by the micromodel (the temperature values are not strongly determinant). Parameters associated with the $X+$, $Y+$, $Y-$, and $SA-$ faces exhibited the weakest recovery due to their limited solar exposure. To date, the solar radiation and thermal imbalance forces have been fit independently and appropriate parameters recovered. However, nonphysical properties could result when the terms are considered jointly. With the delivery of the "as-built" spacecraft models, new micromodels will be generated. These adjusted values will be adopted as nominal values in the actual precision orbit determination computations.

Mission requirements dictate that model performance be evaluated in terms of radial orbit error. In order to quantify the radial orbit error produced by macromodel errors, the following analysis was performed. The micromodel acceleration histories are considered by default to be "truth". Certainly, they are the result of a very rigorous analysis and are the best representation of "truth" that is currently available. Thus, any mismodeling by the macromodel is represented by the

discussed. During this analysis, each of the macro model forces was individually tuned to the micromodel. The Earth albedo and infrared was the exception, which simply uses the solar model tuned parameter values.

For these evaluations, GEODYN was modified to include a routine that does a bilinear interpolation (over β' and Ω) on the micromodel acceleration data for each of the forces considered (solar, albedo, infrared, thermal). Thus, micromodel accelerations were computed at each integration step time within the GEODYN software. The "micromodel GEODYN" version produced four data sets containing true-of-date X, Y, Z data for a 10-day T/P arc, using each of the micromodel accelerations in turn. The particular 10-day arc spans a β' region of 10.5° to 36°, covering the fixed yaw to sinusoidal yaw regime. The analysis is weighted towards the acceleration residuals in this region. Four separate data reduction runs using the macro-model accelerations were made on the four micromodel generated data sets. Thus, for each individual force considered, the only difference in the force modeling between the data generation and data reduction runs in the particular macro-micro model difference. Only the epoch position and velocity of the satellite, a single drag coefficient, and a single solar radiation pressure coefficient were adjusted over the 10-day arc interval. The adjustment of specific macromodel parameters were not part of this study, but are addressed in [49]. The radial RMS orbit error was computed from the residuals of the macromodel-fit orbit to the micro-model-generated orbit.

Table IX gives the modelability and error analysis summary. The RMS radial orbit errors over a 10-day T/P arc for each of the individual macromodel forces is less than 6 cm. It should be stressed that these results were achieved without adjusting T/P macromodel specific parameters, and that the inclusion of these parameters should improve modelability and reduce the orbit errors. The modelability of the along track and cross track albedo and infrared accelerations is poor.

However, the surface properties used to describe the albedo and infrared models were never tuned to the micromodel, and currently the solar model parameter set is employed. The modelability of the accelerations should improve when macromodel parameters are adjusted. Furthermore, the radial component of the albedo and infrared accelerations is an order of magnitude larger than the other components. The modelability of this component is quite good. The along-track thermal acceleration also demonstrates deficiencies due to problems in modeling and tuning the X-plate temperature. Further model tuning is necessary for the X-face. The solar radiation pressure is currently modeled at the 10% level and is anticipated to improve with the tuning of the solar array diffuse and specular reflectivity parameters.

D. Postlaunch Tuning of the Macro Models

It has been shown that the prelaunch "box/wing" macromodels should allow the non-conservative forces to be modeled to a radial accuracy of better than the budgeted 6 cm. However, there is no way to assess the true performance of these models until after launch since we can only compare our models to the spacecraft micromodels, which contain their own errors. Fortunately, any optimism in our analysis of the accuracy of the macromodels should be negated when the macromodels are tuned using real tracking data and telemetered temperature data after launch. The tuning of the macromodels will take place over the same 6 months that the gravity field tuning activities occur. For each plate comprising the box/wing macromodel, a variety of parameters can be estimated to accommodate differences between the micromodel and actual on-orbit performance. The DORIS tracking data will be especially useful for this purpose due to its nearly global coverage. In addition, temperatures of various parts of the spacecraft will be sent down in the telemetry allowing a comparison to the temperatures predicted by the models.

Currently, an intensive study of parameter recoverability and correlation is being pursued in order to determine an ideal parameter set for postlaunch tuning. Once the spacecraft manufacturer supplies the T/P "as-built" models, all of the micromodels will be recomputed and the box/wing parameters will be tailored to these improved solutions. Postlaunch tuning of these models should allow the nonconservative forces acting on T/P to be modeled to the required accuracy.

IV. TRACKING SYSTEM ASSESSMENT

A. Introduction

The mission of T/P requires that the tracking technology be very accurate in the determination of the radial component of the orbit. Satellite laser ranging (SLR) is a very precise technology and is known to provide such accuracy. It has a well established and maintained global network of stations. This "global" nature of the tracking system is crucial to the success of POD since the orbit accuracy requirements (Table IX) apply to the entire trajectory rather than over some limited geographical region.

At the time of the mission planning for T/P, the only other operational and available system with global geodetic capabilities was the TRANET Doppler network. Feasibility studies have shown that this system could not achieve the requirements of POD [44]; it was also of questionable serviceability since the DOD policy was (and is) to replace it with GPS. SLR was at the time the only proven technology both available and capable of meeting our requirements. The Global Positioning System (GPS) was not considered for the role of the primary system because it has not yet been demonstrated as a viable, stable, and reliable user satellite tracking system, even though it has established itself as a precise ground surveying tool. In fact, T/P is to fly the first precise spaceborne GPS tracking system, for which there are great expectations.

SLR has evolved since the 1960's into hardware which is capable of measuring the round trip range to the satellite to individual point accuracies of about a centimeter. This capability was developed, mostly under the auspices of the NASA Crustal Dynamics Project in order to support precision satellite geodesy and geodynamics. These observations have supported investigations involving the rotational dynamics of the Earth, contemporary tectonic plate motions, internal deformation of tectonic plates, regional deformations, and the static and time-varying gravity field of the Earth. The choice of SLR also allows T/P to utilize this well-established geodynamic reference network for precise oceanographic applications.

Recently, a second tracking system to be carried on T/P has demonstrated its capability to precisely track low altitude Earth orbiting satellites. The French DORIS tracking system has flown onboard the SPOT-2 satellite since 1990, and impressive results have been obtained [2], [45]. The DORIS tracking system will provide nearly global tracking coverage for the T/P mission. Unfortunately, the T/P DORIS tracking data, which is downloaded from the satellite to a receiving station near Toulouse France, will probably not be available to the GSFC POD Team as quickly as the SLR data, which is sent electronically to GSFC by the SLR stations. Therefore, preliminary T/P orbits will probably be computed using only the SLR data and DORIS data will be incorporated as it becomes available.

B. Satellite Laser Ranging (SLR)

The principle behind SLR is to measure the time-of-flight of a laser pulse from the observing station to the satellite and back. Onboard the satellite are passive laser corner cube reflectors. All of the active and complicated equipment is located at the ground system. The path through the atmosphere provides a far simpler modeling problem for optical systems than for radiometric type measurements; there is no concern with the ionosphere and the wet component of the troposphere is a much smaller effect. Note however that SLR stations only collect data when the atmosphere is clear; clouds and other weather phenomena prevent the acquisition of data and must be operationally allowed for. The conceptual simplicity of the SLR observation becomes somewhat more complex with the addition of implementation details. The measurement desired is the time-of-flight from the optical center of the observing telescope and back. The epoch time of the observation is

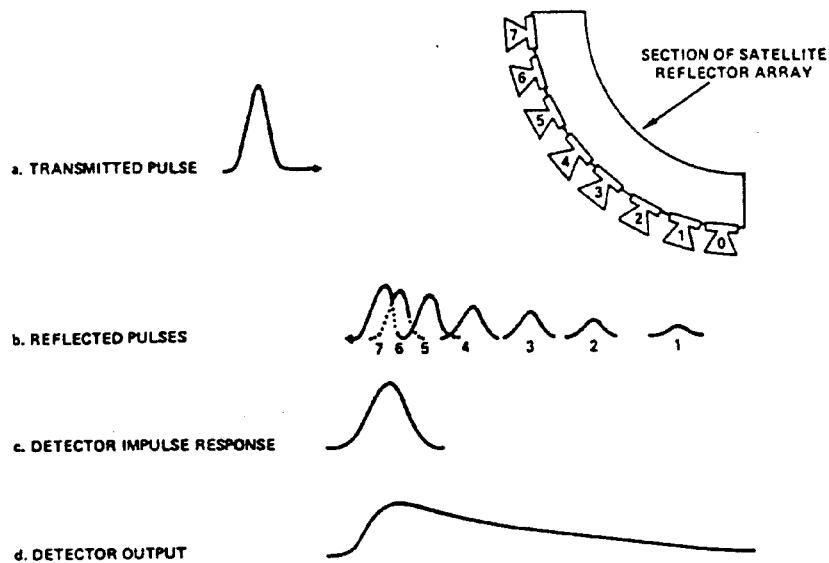


Fig. 7. Illustration of LRA-induced pulse spreading (from [47]).

required. A real optical pulse is used. The corner cubes on the satellite are not at the center of mass of the spacecraft and are generally tilted with respect to the line of sight. These complexities and others are dealt with in practice through a combination of modeling and calibration. A detailed description of these matters is found in Degnan [1].

The raw SLR measurement contains the sum of the round trip travel time and a system bias which is defined by calibration procedures at the time of the observations. Also, the convention in processing satellite tracking data is to modify the observable to refer to the center of mass of the spacecraft and to remove the path lengthening due to media propagation delays. These preprocessing corrections are well understood and permit the required accuracy goals for T/P to be achieved.

The correction to the center of mass of the spacecraft is derived accurately from the satellite physical measurements, information about the instantaneous attitude state, prelaunch calibration measurements, and specific information about the quality and manufacturing of the corner-cube-reflectors (CCRs). Once these quantities have been established, the correction is derived in the form of a time series to be applied to the observed ranges.

The pre-launch calibration is an important factor in ensuring a high quality, reliable center-of-mass (CM) correction. Each CCR has its own optical inhomogeneities and imperfections, and the response of the full aggregate of the multiple CCRs comprising the laser retroreflector array (LRA) must be mapped. The process requires the physical measurement of the CCR response to laser pulses with the same shape, wavelength, amplitude and power as they will encounter in practice after the launch of the satellite. The calibration measurements are required both at the individual CCR level and for the full LRA. Fig. 7 illustrates the general process behind the array response. A Gaussian pulse is reflected off the array. The detector input is the sum of the reflected pulses from each separate CCR

taking into account the fact that the detector is in the far field (Fraunhofer diffraction). The detector response, because of its bandwidth, implicitly smooths the pulse train resulting in the final "pulse broadened" output waveform at this particular view. Finally, while there is only one target LRA on the satellite, each individual ground system has its own pulse width and detection mechanism as well as laser wavelength. These ground system characteristics define how the laser will respond to the input waveform and thus are required to derive the actual CM correction. Because the adopted network comprises systems with varied characteristics, more than one series of CM corrections is required.

The LRA designed for T/P produces a much more complicated return than other geodetic satellites such as LAGEOS. This complex return introduces an additional error source in the ranging process: a variable lidar cross-section. This in turn, coupled with the various aspect angles from which the LRA will be viewed from the ground, introduces possible biases that depend on the number of photoelectrons reaching the receivers. Ground testing and careful far-field diffraction pattern (FFDP) modeling at GSFC will limit LRA-induced biases to the 5 mm to 1 cm level.

The propagation media corrections for SLR are quite simple and well established in the literature [46]. Due to the use of frequencies in the visible part of the spectrum, we only need to concern ourselves with the correction for tropospheric refraction (wet and dry component combined). Even this correction is only mildly affected by the water vapor content of the atmosphere, unlike the case of radio frequencies where that is the most serious effect. Nevertheless, the available models are only sufficient for elevations above 10–15°. The Marini and Murray model, which uses site-observed meteorology, has proven quite adequate in the reduction of LAGEOS laser ranging data. Since LAGEOS is a much "cleaner" spacecraft and its orbit quite stable and insensitive to less well modeled

TABLE X
TOPEX/POSEIDON SLR TRACKING NETWORK STATION LOCATIONS

Station Num.	Latitude			Longitude			Height (m)	Station Name
	°	'	"	°	'	"		
7105	39	1	14	283	10	20	19.16	GREENBELT
7210	20	42	26	203	44	39	3067.53	MAUI
7109	39	58	30	239	3	19	1106.35	QUINCY
7110	32	53	30	243	34	38	1838.96	MONUMENT PEAK
7080	30	40	49	255	59	5	2004.27	MCDONALD OBS.
7122	23	20	34	253	32	27	30.82	MAZATLAN
7840	50	52	3	0	20	10	75.39	HERTMONCEUX
7834	49	8	42	12	52	41	661.14	WETTZELL
7939	40	38	56	16	42	17	535.81	MATERA
7530	31	43	21	35	5	19	774.41	BAR GIORA
7838	33	34	40	135	56	13	99.41	SIMOSATO
7090	-29	2	47	115	20	48	241.36	YARAGADEE
7843	-35	38	11	148	56	22	1349.92	ORRORAL
7123	-16	44	1	208	58	32	45.31	HUAHINE ISLAND
7097	-27	8	52	250	36	59	117.29	EASTER ISLAND
7403	-16	27	57	288	30	25	2492.34	AREQUIPA
7401	-30	10	21	289	11	60	2156.72	CERRO TOLOLO
7837	31	5	51	121	11	30	28.55	SHANGHAI

perturbations, it provides a test-bed for such models. In that respect, the procedure used for LAGEOS seems to be quite adequate for the T/P tracking as well. Quantitatively, we do not expect the model to introduce systematic errors of more than 1 mm at 20° elevations, well below 0.1 mm near zenith. Similarly, random errors about these biases, mostly due to the short period and local variations in the lower layer of the atmosphere, are not expected to exceed 3 mm and 1 mm, respectively, at the above elevations.

Below 15° elevation, significant errors can be anticipated unless techniques such as adjusting a scale-factor estimation on the zenith delay, are applied. Furthermore, there is introduced a greater sensitivity to the assumption of spherical symmetry in the atmosphere. However, there are only experimental models that can consider the effect of horizontal gradients in the atmosphere and they require the existence of rather extensive regional networks collecting surface meteorological information. It is simply more practical to adopt a conservative 15° elevation cutoff criterion.

The adopted SLR tracking network comprises three sets of stations: NASA-owned and operated sites, university operated NASA sites, and international cooperating sites. After discussions and studies of the network requirements, the Crustal Dynamics Project Global Laser Tracking Network group proposed a selection of sites from all three types to form the T/P tracking network. These sites are listed in Table X and their geographic distribution are shown in Fig. 8. Simulations have shown that this network does provide the necessary accuracy and coverage to provide orbits of the required accuracy for T/P. With the exception of the tracking site at Mazatlan, Mexico, all of the T/P Project requested sites are in full readiness. Mazatlan has since been deactivated and it thus will only participate when visited by a transportable laser ranging system (TLRS). This should not significantly degrade the anticipated accuracy of the T/P orbit. Additionally, new systems are becoming available and we can expect that in

practice we will have enough global redundancy in the network to account for unpredictable data outages at the nominal sites due to weather conditions.

All of the sites have undergone significant upgrades since the time of selection, especially those owned and operated by NASA. The current precision of these systems (which depends on the target also) is on the order of a few mm, while their accuracy is at the 1 cm level. Recent side-by-side system collocation campaigns have demonstrated that the biases with these systems do not exceed 1 cm. There is little variation in site performance during day-tracking versus night-tracking. In terms of reliability, the history on LAGEOS indicates that about 10% of the possible passes were not tracked due to equipment, or other subsystem failure. This does not include weather, which is by far the dominant reason for failure to track a particular pass. A typical variation would range from a 20% to a 80% outage with a strong seasonal dependence, averaging 40% over the year. This measure is of course extremely site dependent. A detailed description of these assessments, particularly as they relate to T/P, may be found in Murdoch and Decker [47].

C. The DORIS Contribution

The Poseidon portion of the T/P mission includes tracking by a new French system, the Doppler Orbitography and Radiopositioning Integrated by Satellite (DORIS) system. DORIS is an inverted TRANET type system in that the observations of a network of ground beacons are made on-board the spacecraft and downlinked at a master control site. In contrast to the laser system, most of the complexity is associated with the on-board package. High performance quartz ultra-stable oscillators are at the heart of the system design; performance specifications require oscillator stability of 5×10^{-13} over 10 seconds. Like TRANET, this is a two-frequency system, but uses higher frequencies (2 GHz and 400 MHz) to more precisely model the ionospheric effects (these differences address the major

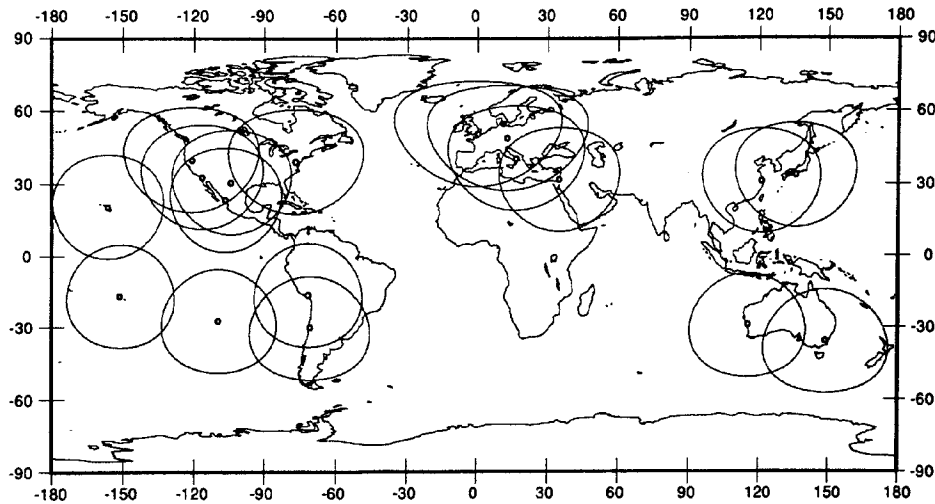


Fig. 8. Locations and visibility masks of the SLR stations comprising the T/P SLR tracking network (15° Elevation Cutoff).

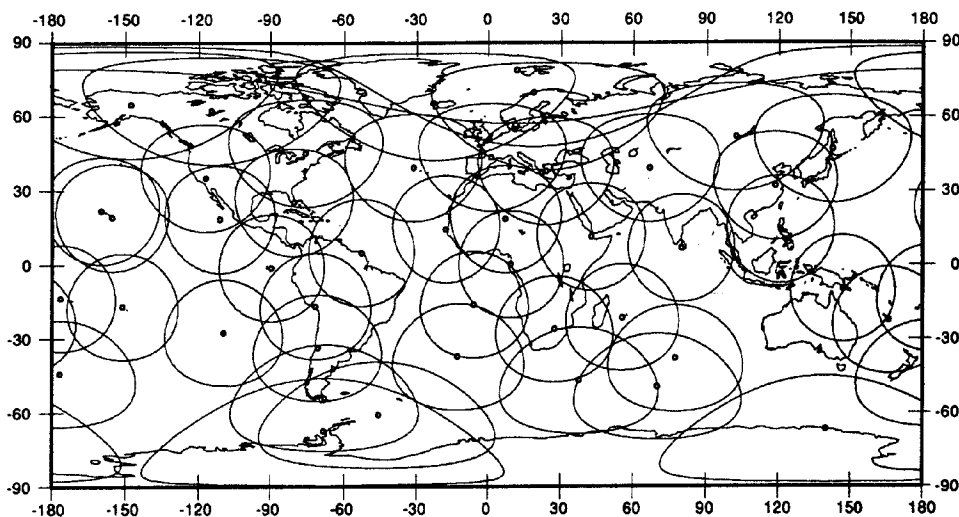


Fig. 9. Locations and visibility masks of the DORIS tracking stations (15° elevation cutoff).

limitations which were known in TRANET). The DORIS measurements on SPOT-2 have a theoretical 0.3 mm/s noise over a 9-second destruct count interval; 0.5 mm/s is actually observed. This DORIS measurement is roughly equivalent to a 5 cm ranging system which has an unknown bias.

The principle behind the DORIS measurement is the traditional Doppler effect, where the measurement is the count of the number of cycles of an observed signal over a designated time interval. This observable is directly related to the change in range over the interval. In parallel with the SLR situation, the actual implementation is fraught with complexities; how the epoch timing occurs, what time systems are used, where the antennas are on the spacecraft, and how the ground beacon is characterized. The preprocessing corrections to modify the observable to refer to the center of mass of the spacecraft and to remove the path lengthening due to media propagation delays are required as they are in the SLR

case. The electronic analog to the center of the laser array is the antenna phase center; the media propagation delays include ionospheric effects as well as a relatively poorly modeled "wet" tropospheric term. However, given the wealth of tracking data provided by these all weather systems, it is routine to adjust a refraction scaling parameter over each 10–15 minute data pass. Note that the ground meteorology from the beacon is also used.

The DORIS network is shown in Fig. 9, and the ground beacon sites are tabulated in Table XI. Reliability does not seem to be an issue in the sense that the ground beacons are simple and easy to maintain, and, because the system is electronic, it will take data in all sorts of weather conditions. DORIS was not an operational system in our mission planning phase, but flew recently as a successful experiment on SPOT-2. GSFC was able to participate in the checkout of the DORIS system, using the data both to compute precision orbits and to

TABLE XI
DORIS TRACKING NETWORK STATION LOCATIONS

Station		Latitude			Longitude			Height (m)	Station Name
Num	Desig.	°	'	"	°	'	"		
4002	TLSA	43	33	29	1	28	52	208.91	TOULOUSE
4005	TRIA	-37	3	55	347	41	15	35.33	TRISTAN DA CUN
4006	META	60	14	31	24	23	4	62.87	METSAHOVI
4008	AMSA	-37	47	54	77	34	17	65.11	AMSTERDAM
4009	KERA	-49	21	7	70	15	46	66.17	KERGUELEN
4010	GOLA	35	19	53	243	6	30	898.61	GOLDSTONE
4012	REUA	-21	12	30	55	34	18	1561.65	LA REUNION
4013	LIBA	0	21	15	9	40	20	37.66	LIBREVILLE
4016	KRUA	5	6	50	307	21	18	121.50	KOUROU
4017	RIOA	-53	47	9	292	14	54	33.66	RIO GRANDE
4018	DAKA	14	43	55	342	33	60	43.07	DAKAR
4019	HBKA	-25	53	14	27	42	27	1563.31	HARTEBEESTHOEK
4020	SPIA	78	55	24	11	55	54	54.43	NY-ALESUND
4022	MARA	-46	52	44	37	51	25	93.40	MARION ISLAND
4023	RICA	25	37	29	279	36	52	-18.69	RICHMOND
4025	DJIA	11	31	35	42	50	48	717.21	DJIBOUTI
4027	HUAA	-16	44	1	208	57	32	46.17	HUAHINE
4029	TLTA	43	33	39	1	29	0	203.98	TOULOUSE
4035	ARLA	18	44	10	7	22	38	446.79	ARLIT
4036	NOUA	-22	16	10	166	24	37	89.90	NOUMEA
4037	WALA	-13	15	57	183	49	14	158.23	WALLIS
4038	SANA	-33	23	45	289	27	47	895.99	SANTIAGO
4039	CHAA	-43	57	26	183	25	41	69.59	CHATHAM
4040	SOCA	18	43	35	249	2	46	13.03	SOCORRO
4041	EASA	-27	8	52	250	36	59	120.89	EASTER ISLAND
4042	ADEA	-66	39	46	140	0	5	2.26	TERRE ADELIE
4043	HELA	-15	56	32	354	19	57	454.29	SAINTE-HELENE
4045	PURA	32	4	2	118	49	29	266.08	PURPLE MOUNTAIN
4046	AREA	-16	27	57	288	30	25	2494.58	AREQUIPA
4047	DIOA	38	4	42	23	55	58	514.29	DIONYSOS
4048	OTTA	45	23	59	284	17	39	113.94	OTTAWA
4050	SIGA	-60	42	32	314	24	16	31.01	SIGNY ISLAND
4051	YELA	62	28	51	245	31	12	186.83	YELLOWKNIFE
4053	FLOA	39	27	18	328	52	20	81.25	FLORES
4054	TROA	69	39	46	18	56	21	136.65	TROMSO
4055	MORA	-9	26	10	147	11	9	156.19	PORT MORESBY
4102	DJMB	11	37	2	42	33	21	463.09	DJIBOUTI
4103	DJCB	11	32	6	42	26	43	369.63	DJIBOUTI
4881	SAKA	47	1	47	142	43	0	91.43	SAKHALINSK
4882	KITA	39	8	1	66	53	5	630.81	SAMARKAND
4883	BADA	51	46	11	102	14	6	812.84	BAIKAL
4884	MANA	14	32	8	121	2	28	87.78	MANILLE
4885	COLA	6	53	31	79	52	27	-76.09	COLOMBO
4886	KOKA	22	7	23	200	20	5	1166.18	KOKEE PARK
4887	REYA	64	9	4	338	0	17	96.27	REYKJAVIK
4888	FAIA	64	58	18	212	29	15	351.09	FAIRBANKS
4901	HVOA	19	25	14	204	42	44	1269.41	
4902	GALA	0	54	3	270	23	2	4.07	
4903	ROTA	-67	34	10	291	52	32	27.78	
4904	SODA	18	43	40	249	2	53	19.84	SOCORRO

improve the gravity field. The radial accuracy of 5-day orbits was formally assessed as being better than 20 cm on this 800 km altitude orbit [45]. Without supporting altimetry and/or laser tracking, it is difficult to confirm this evaluation. For T/P, the promise is clear.

D. Summary

The global SLR tracking network is ready to undertake the precision tracking of T/P in support of its oceanographic and geodetic goals. The DORIS tracking system will now also be used for the baseline T/P tracking support, and it will play a significant role in the orbit computations. DORIS data,

in combination with SLR data, will enable the orbit to be determined to a high level of accuracy given the accuracy of the supporting force models. While DORIS is of lesser accuracy than SLR data and is an inherently biased type, it has significantly better global coverage; almost continuous coverage can be obtained. When used in conjunction with the SLR data, the nonconservative forces will be better resolved. The T/P mission has been designed such that orbits with the required radial accuracy could be computed using either SLR tracking data or DORIS tracking data. However, given the realities of the differences between planned and actual missions, and that the real spacecraft is a much more complicated shape with a much more complicated attitude control system

than originally envisioned, the best orbits will be computed using both SLR and DORIS tracking data. Should the GPS experiment on T/P be successful, the combination of the three techniques could allow not only the computation of orbits of unprecedented accuracy, but also the improvement of the long-wavelengths of the Earth's gravity field.

V. SUMMARY OF THE EXPECTED POD ACCURACY FOR TOPEX/POSEIDON

We have examined each of the components required for the computation of precise orbits for the T/P spacecraft: gravity field modeling, nonconservative force modeling, and satellite tracking technologies. Clearly the availability of precise globally distributed satellite tracking data is the most important component, since inadequacies in the force models can at least partially be offset by using the tracking data to improve the parameters defining the models. The baseline SLR tracking system provides cm level range measurements to the spacecraft and may be the best system for defining the location of the orbit relative to the center-of-mass of the Earth, which is important for studies of global sea level rise. However, should a problem arise with the gravity model or the box/wing macromodel describing the nonconservative forces, the DORIS tracking data will serve an important role due to its superior global coverage. If there should be a problem with either of these two tracking systems, the use of GPS or TDRSS tracking would help fill in the resulting gaps. GPS tracking is an experiment of T/P, but it may well prove to be the best tracking system on the satellite, since true continuous tracking is obtained. TDRSS tracking will mainly be used for orbit maintenance and planning spacecraft maneuvers, which have much lower accuracy requirements. However, this system could also be used if a problem develops with one of the other more precise tracking systems.

The error covariance of the GEM-T3 gravity model currently predicts radial orbit errors for T/P of 7 cm RMS. While this is well within the T/P requirements, error covariance analyses have traditionally been found to be optimistic due to the presence of unmodeled measurement and modelling errors not represented in the covariance analysis. However, if the errors predicted by the GEM-T3 covariance are somewhat optimistic, any difference with the actual errors will most likely be overcome during the iteration of the gravity model or during the postlaunch tuning of the reiterated model with T/P tracking data. Thus, while the radial orbit errors caused by the gravity field are likely to be the largest error source in the orbit computations, the POD Team is confident that the 10 cm requirement can be met. Errors in modeling the time variations in the gravity field caused by the tides are also of concern to the POD team, but a combination of postlaunch tuning and improvements in the background tide models should allow the 3 cm requirement to be met. It should be noted, however, that current predictions of the T/P radial orbit error due to errors in the long period tides are at about the 3 cm level. Thus some improvements in this area will be needed, and is expected.

Errors in modeling the nonconservative forces acting on the spacecraft may be the biggest prelaunch concern for the

T/P POD Team. Prelaunch modeling studies have shown the errors in modeling solar and Earth radiation pressure and thermal imbalances will approach the allotted 6 cm. After launch, very few model parameters can be directly monitored on the spacecraft for variations from the prelaunch values. The attitude of the spacecraft can be checked through telemetry and the temperature of certain parts of the spacecraft can be verified, but accurate modeling of the nonconservative forces will largely depend on the *a priori* box/wing macro models. Tuning of the box/wing parameters after launch should considerably reduce any large errors that may remain in the macro model. Another concern is the variation in the properties of the external spacecraft material over time, which is nearly impossible to monitor. After a year or more in orbit, the nonconservative forces acting on the spacecraft may have a quite different character simply due to the degradation of the exposed surfaces on the satellite. Should the modeling of the nonconservative forces become a problem, empirical parameters could be estimated in the orbit determination process to help remove much of the resulting orbit error. This technique has been used with considerable success on other altimetric satellites such as Seasat and Geosat [48]. However, this technique requires tracking data with good global distribution. Thus the DORIS tracking data would be indispensable in this event.

We have mentioned some of the possible problems with the POD for T/P in this final section in order to emphasize the fact that, as good as our force models have become, simply meeting the error requirements may not be sufficient if an off-nominal condition occurs on the spacecraft. Therefore, we will continue to improve our models, beyond the error requirements if necessary, in order to provide the most accurate ephemeris possible for the T/P spacecraft.

REFERENCES

- [1] J.J. Degnan, "Satellite laser ranging: Current status and future prospects," *IEEE Trans. Geosci. Remote Sensing*, vol. GE-32, pp. 398-513, 1985.
- [2] A. Cazenave *et al.*, "Positioning results with DORIS on SPOT-2 after first year of mission," *J. Geophys. Res.*, vol. 97, no. B5, pp. 7109-7119, 1992.
- [3] J.T. Wu and T.P. Yunck, "TOPEX orbit determination and gravity recovery using global positioning system data from repeat orbits," *J. Geophys. Res.*, vol. 97, no. B2, pp. 1973-1979, 1992.
- [4] A.J. Schanzle *et al.*, "Orbit determination support of the ocean topography experiment (TOPEX)/Poseidon operational orbit," *Flight Mechanics/Estimation Theory Symposium*, NASA/Goddard Space Flight Center, 1992.
- [5] B.H. Putney, "GEODYN II system description," NASA/Goddard Space Flight Center, STX Contractor Report 1991.
- [6] F.J. Lerch *et al.*, "Gravity model development from Lageos," *Geophys. Res. Lett.*, vol. 9, pp. 1263-1266, 1982.
- [7] J.G. Marsh *et al.*, "A new gravitational model for the earth from satellite tracking data: GEM-T1," *J. Geophys. Res.*, vol. 93, pp. 6169-6215, 1988.
- [8] J.G. Marsh *et al.*, "The GEM-T2 Gravitational Models," *J. Geophys. Res.*, vol. 95, no. B13, pp. 22043-22071, 1990.
- [9] F.J. Lerch *et al.*, "Geopotential models of the Earth from satellite tracking altimeter, and surface gravity observations: GEM-T3 and Gem-T3S," NASA/Goddard Space Flight Center, Tech. Memo. 104555, Jan. 1992.
- [10] K.F. Walker, "Report by the subcommittee on the intercomparison and merging of geodetic data of the TOPEX/Poseidon Science Working Team," Delft University of Technology, May, 1990.

- [11] F. J. Lerch *et al.*, "An improved error assessment for the GEM-T1 gravitational model," *J. Geophys. Res.*, vol. 96, no. B12, pp. 20023–20040, 1991.
- [12] F. J. Lerch *et al.*, "Direct calibration of GEM-T1 with 1071 5×5 degree mean gravity anomalies from altimetry," *Manuscripta Geodaetica*, vol. 16, pp. 141–147, 1991.
- [13] F. J. Lerch *et al.*, "New error calibration tests for gravity models using subset solutions and independent data," *Geophys. Res. Lett.*, in review, 1992.
- [14] W. M. Kaula, *Theory of Satellite Geodesy*. Waltham, MA, Blaisdell, 1966.
- [15] B. D. Tapley and G. W. Rosborough, "Geographically correlated orbit error and its effect on satellite altimeter missions," *J. Geophys. Res.*, vol. 90, pp. 11817–11831, 1985.
- [16] O. L. Colombo, "Altimetry, Orbits, and Tides," NASA, Tech. Memo. 86180, 1984.
- [17] T. E. Engelis, "On the simultaneous improvement of a satellite orbit and determination of sea surface topography using altimetric data," *Manuscripta Geodetica*, vol. 13, pp. 180–190, 1988.
- [18] C. A. Wagner, "Radial variations of a satellite due to gravitational errors: implications for satellite altimetry," *J. Geophys. Res.*, vol. 90, pp. 3027–3036, 1985.
- [19] S. Levitus, "Climatological atlas of the world ocean," NOAA, Professional Paper 13, 1982.
- [20] G. W. Rosborough, "Satellite orbit perturbations due to the geopotential," Center for Space Research, Tech. Memo. 86-1, 1986.
- [21] J. C. Ries *et al.*, "Progress in the determination of the gravitational coefficient of the Earth," *Geophys. Res. Lett.*, vol. 19, no. 6, pp. 529–531, 1992.
- [22] D. D. McCarthy, "IERS standards," Observatoire de Paris, IERS Tech. Note 3, 1989.
- [23] D. E. Smith *et al.*, "Tectonic motion and deformation from satellite laser ranging to LAGEOS," *J. Geophys. Res.*, vol. 95, no. B13, pp. 22013–22041, 1990.
- [24] C. Demets *et al.*, "Current plate motions," *Geophysical Journal International*, vol. 101, pp. 425–478, 1990.
- [25] J. C. Ries *et al.*, "Effect of general relativity on a near-Earth satellite in the geocentric and barycentric reference frames," *Phys. Rev. Lett.*, vol. 61, no. 8, pp. 903–906, 1988.
- [26] C. Huang *et al.*, "Relativistic effect for near-Earth satellite orbit determination," *Cel. Mech. Dyn. Astro.*, vol. 48, pp. 167–185, 1990.
- [27] P. C. Knocke *et al.*, "Earth radiation pressure effects on satellites," *AIAA/ASS Astrodynamics Conference* (KalisPELL, MT) pp. 577–587, 1988.
- [28] A. E. Hedin, "MSIS-86 thermospheric model," *J. Geophys. Res.*, vol. 92, no. A5, pp. 4649–4662, 1987.
- [29] D. C. Christodoulidis *et al.*, "Observed tidal braking in the Earth/moon/sun system," *J. Geophys. Res.*, vol. 93, pp. 6216–6236, 1988.
- [30] J. M. Wahr, "The tidal motions of a rotating, elliptical, elastic, and oceanless Earth," Ph.D. dissertation, The University of Colorado, 1979.
- [31] J. M. Wahr, "Body tides on an elliptical, rotating, elastic, and oceanless Earth," *Geophys. J. R. Astron. Soc.*, vol. 64, pp. 677–703, 1981.
- [32] J. M. Wahr, "The forced nutations of an elliptical, rotating, elastic, and oceanless Earth," *Geophys. J. R. Astron. Soc.*, vol. 64, pp. 705–727, 1981.
- [33] O. L. Colombo, personal communication, 1989.
- [34] S. Casotto, "Ocean tide models for TOPEX precise orbit determination," Ph.D. dissertation, Center for Space Research, The University of Texas at Austin, 1989.
- [35] C. Perrygo, "TOPEX Satellite yaw maneuvers," Fairchild Space Co., IOC REF: 968:SE:87-074, Nov. 11, 1987.
- [36] D. Zimbelman, "Final version of TOPEX EULERC subroutine," Fairchild Space Co., IOC REF:GNC:TOPEX:89-229, Oct. 17, 1989.
- [37] G. W. Rosborough and P. Antreasian, "Radiation force modeling for the TOPEX/Poseidon spacecraft," *AAS/AIAA Astrodynamics Conference*, 1990.
- [38] P. G. Antreasian and G. W. Rosborough, "Prediction of radiant energy forces on the TOPEX/Poseidon spacecraft," *J. Spacecraft and Rockets*, vol. 29, no. 1, pp. 81–90, 1992.
- [39] P. G. Antreasian, "Precision radiation force modeling for the TOPEX/Poseidon mission," Ph.D. dissertation, Dept. of Aerospace Engineering Sciences, The University of Colorado, Boulder, CO, 1992.
- [40] J. A. Marshall *et al.*, "Modeling radiation forces acting on satellites for precision orbit determination," *AAA/AIAA Astrodynamics Conference*, Durango, CO, 1991.
- [41] J. A. Marshall *et al.*, "Modeling of radiation forces acting on satellites for precision orbit determination," NASA/Goddard Space Flight Center, Tech. Memo. 104564, June 1992.
- [42] A. Milani, *et al.*, *Non-Gravitational Perturbations and Satellite Geodesy*. Bristol, England. Adam Hilger, 1987.
- [43] P. Knocke and J. C. Ries, "Earth radiation pressure effects on satellites," Center for Space Research, Tech. Memo. 87-01, Sept. 1987.
- [44] J. C. Ries *et al.*, "Analysis of TRANET-II tracking data for Geosat," Center for Space Research, Tech. Memo. 86-01, Aug. 1986.
- [45] R. S. Nerem *et al.*, "An evaluation of the DORIS tracking system on SPOT-2," *International DORIS Orbit Computation Workshop* (Toulouse, France), edited by F. Nouel, CNES, 1991.
- [46] J. Marini and C. Murray, "Correction for laser range tracking for atmosphere refraction at elevation above 10 degrees," NASA/Goddard Space Slight Center, Tech. Memo. X-70555, 1973.
- [47] A. Murdoch, and W. Decker, "Crustal dynamics laser ranging network preliminary TOPEX/Poseidon laser network support plan," NASA/Goddard Space Flight Center, CDSLR-03-002, 1989.
- [48] R. S. Nerem *et al.*, "Determination of the ocean circulation using geosat altimetry," *J. Geophys. Res.*, vol. 95, no. C3, pp. 3163–3179, 1990.
- [49] S. B. Luthcke and J. A. Marshall, "Nonconservative force model parameter estimation strategy for TOPEX/POSEIDON precision orbit determination," NASA Tech. Memo. 104575, Nov. 1992.